

Electronic Structure and Phase Transition in V_2O_3 : Importance of 3d Spin-Orbit Interaction and Lattice Distortion

Arata TANAKA

Department of Quantum Matter, ADSM
Hiroshima University, Higashi-Hiroshima 739-8530, Japan

(Received)

The 3d electronic structure and phase transition in pure and Cr doped V_2O_3 are theoretically investigated in relation to the 3d spin-orbit interaction and lattice distortion. A model consisting of the nearest-neighbor V ion pair with full degeneracy of the 3d orbitals is studied within the many-body point of view. It is shown that each V ion with $S = 1$ spin state has a large orbital magnetic moment $\sim 0.7\mu_B$ and no orbital ordering occurs in the antiferromagnetic insulating (AFI) phase. The anomalous resonant Bragg reflection found in the AFI phase is attributed to the magnetic ordering. In the AFI and paramagnetic insulating (PI) phases, Jahn-Teller like lattice instability leads to tilting of the V ion pairs from the corundum c -axis and this causes large difference in the orbital occupation between the paramagnetic metal and the insulating phases, which is consistent with linear dichroic V 2p XAS measurements. To understand the AFI to PI transition, a model spin Hamiltonian is also proposed. The transition is found to be simultaneous order-disorder transition of the magnetic moments and tilting directions of the V ion pairs. Softening of elastic constant C_{44} and abrupt change in short range spin correlations observed at the transition are also explained.

KEYWORDS: V_2O_3 , electronic structure, phase transition, lattice distortion, orbital ordering, spin-orbit interaction, orbital moment, resonant x-ray scattering, V 2p XAS

§1. Introduction

The metal-insulator (Mott) transition in V_2O_3 have been extensively studied ever since Mott suggested the possibility of the localization of electrons driven by Coulomb repulsion.¹⁾ Above the transition temperature $T_N \sim 155$ K, the material is paramagnetic metal (PM) and has the corundum structure with the trigonal symmetry (space group $R\bar{3}c$). Below T_N , it is an antiferromagnetic insulator (AFI) and the lattice distortion to the monoclinic structure ($I2/a$) takes place.²⁾ Cr doped alloys $(V_{1-x}Cr_x)_2O_3$ exhibit also interesting features.³⁻⁷⁾ For $0.005 < x < 0.018$, at a temperature above the AFI \rightarrow PM transition, the material further undergoes a PM to paramagnetic insulator (PI) phase transition with no change in the crystal structure. For much higher Cr concentration $x > 0.018$, the PM phase disappears and a AFI \rightarrow PI transition takes place.

Although V_2O_3 and its alloys are often referred to a typical example of the Mott-Hubbard system, there are experimental facts showing the complex aspects of these materials, which can not be explained by the simple single-band Hubbard model. In the AFI phase, they exhibit unusual magnetic order, which breaks corundum trigonal symmetry.⁸⁾ Neutron scattering experiments have been performed by Bao *et al.* and abrupt change in spatial spin correlation functions has been reported both at the AFI \rightarrow PM and the AFI \rightarrow PI transitions.^{9,10)} This switching of spin correlation indicates that the phase transitions can not be considered as usual order-disorder magnetic transition. Softening of the C_{44} elastic constant has been observed in ultrasonic wave¹¹⁾ and neu-

tron scattering¹²⁾ experiments at the AFI \rightarrow PI transition, indicating nearly second order feature of this phase transition as well as strong electron-lattice coupling.

Even now, the electronic structure of these materials are still controversial problem and above experimental facts suggest that much realistic model including the orbital degeneracy of the 3d orbital and the lattice distortion is necessary to explain them. In V_2O_3 , the O_h crystal field splits the 3d orbitals of each V ion into two fold e_g and three fold t_{2g} orbitals and the t_{2g} orbitals are further separated into low laying two fold e^π and non-degenerate a_1 orbitals by small trigonal field. In localization limit, two 3d electrons in the V^{3+} ion are accommodated in the lowest e^π orbitals with $S = 1$ spin state. Castellani *et al.* have proposed a model including these e^π and a_1 orbitals.¹³⁾ In the corundum structure, two V ions forms pairs along c -axis and in their model, the a_1 orbitals on two V ions of the pair forms molecular orbitals. The bonding a_1 orbital accommodates two electrons out of four in the pair and remaining two electrons occupies one of e^π orbital in each V ions, resulting in $e^\pi a_1$ configuration with $S = 1/2$ spin state in each V ion. They also propose a long-range ordering of orbital occupation in the two fold e^π orbital to explain the complex antiferromagnetic ordering in the AFI phase.

However, recent measurements on the linear dichroism of V 2p x-ray absorption spectra (XAS) in V_2O_3 have revealed that the 3d electron configuration is not $S = 1/2$ $e^\pi a_1$ but mixture of $e^\pi e^\pi$ and $e^\pi a_1$ with $S = 1$ Hund's rule spin state.¹⁴⁾ In addition, large differences in $e^\pi e^\pi$ to $e^\pi a_1$ ratio have been found among the AFI, PI and PM phases. Indeed, such $S = 1$ Hund's rule spin state is

also obtained in recent “LDA+U”^{15,16)} band structure calculation,¹⁷⁾ in which a $S = 1 e^{\pi}e^{\pi}$ ground state having experimentally observed antiferromagnetic order with no orbital degeneracy is favorable for the low temperature monoclinic phase. Mila *et al.* have proposed a model with a large intraatomic exchange interaction.^{18,19)} In this model, spin state in each V ion remains being $S = 1$ even with strong hybridization between a_1 orbitals. The electronic state of the V ion pair is described as a superposition of two configurations with equal weight: $e^{\pi}a_1; e^{\pi}e^{\pi}$ (the $e^{\pi}a_1$ configuration in one of V ion and the $e^{\pi}e^{\pi}$ configuration in the other) and $e^{\pi}e^{\pi}; e^{\pi}a_1$. In this model, two fold orbital degeneracy is present in this V_2 molecular orbital and the complex antiferromagnetic order in the AFI phase is stabilized with a ferro-type order of this V_2 molecular orbital.

Paolasini *et al.* have performed resonant x-ray scattering experiments (RXS) at the V K -edge on V_2O_3 and they insisted that resonant Bragg peaks observed in the AFI phase are due to the $3d$ orbital ordering.^{20,21)} However, Lovesey and Knight have argued that the resonant Bragg peaks arise from the ordered orbital magnetic moments of the V ions.²³⁾ Indeed, nonresonant magnetic scattering has been also measured and a large contribution from the orbital magnetic moment to the total magnetic moment $M_L/M_S \sim -0.3$ was found.²⁰⁾ It is thus important to know how the $3d$ spin-orbit interaction affects the $3d$ electronic structure of V_2O_3 . Since this interaction couples spin and orbital degrees of freedom, in the presence of a large orbital angular momentum, no orbital ordering is expected in the AFI phase. In above mentioned theories on the electronic structure of V_2O_3 , however, the effects of the $3d$ spin-orbit interaction in the V ions is presumed to be small.

The purpose of this paper is to clarify the effects of the $3d$ spin-orbit interaction and the lattice distortion on the $3d$ electronic structure and the phase transitions of the pure and Cr doped V_2O_3 . To this end, first of all, a V ion pair model similar to that proposed by Mila *et al.* will be considered taking into account the $3d$ spin-orbit interaction in § 2. With the $3d$ spin-orbit interaction, no orbital ordering is expected in the AFI phase and instead of this, a large orbital magnetic moment $\sim 0.7\mu_B$ is induced in the ground state. The relation between the monoclinic distortion and the magnetic anisotropy and difference in the configuration of the $3d$ electrons between the AFI and PM phases will be also discussed. Second, interaction between the electronic state of the V ion pair and local lattice distortion caused by displacement of the pair will be discussed in § 3. It will be shown that Jahn-Teller like lattice instability occurs when the energies of the $e^{\pi}a_1; e^{\pi}e^{\pi}$ ($e^{\pi}e^{\pi}; e^{\pi}a_1$) and $e^{\pi}e^{\pi}; e^{\pi}e^{\pi}$ states are nearly degenerate. Third, relation between the magnetic ordering and the lattice distortion in the AFI phase and also the mechanism of the AFI \rightarrow PI transition will be discussed in § 4. For this purpose, an effective Hamiltonian with exchange interaction between the V ion pairs including lattice distortion effects is proposed. Softening of the elastic constant C_{44} and abrupt change in short range spin correlation functions observed at the AFI to PI transition are reproduced with the model. Finally, to

confirm the validity of the present model, recent experiments on RXS and the linear dichroic V $2p$ XAS spectra are analyzed in § 5 and § 6, respectively. The experimental results are well explained within the present model.

§2. V ion Pair Model

2.1 Model Hamiltonian

Each V ion in the corundum structure of V_2O_3 is octa-

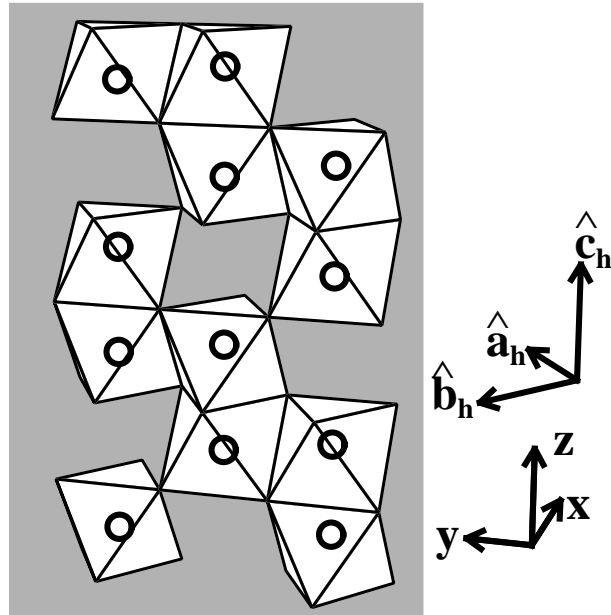


Fig. 1. Corundum structure of V_2O_3 . Each V ion (open circles) is octahedrally surrounded by six oxygen ions (octahedra). Along the c_h axis, the V ion pairs surrounded by the face-sharing two oxygen-octahedra are seen whereas in a_h - b_h plane, each V ion has three neighbors with edge-sharing oxygen-octahedra.

hedrally surrounded by six oxygen ions (see Fig. 1). An octahedral crystal field and hybridization between the V $3d$ and O $2p$ orbitals split the energy level of the $3d$ orbital into the e_g and t_{2g} levels and the low laying t_{2g} orbitals accommodate two electrons in each V^{3+} ion. A small trigonal distortion of the oxygen octahedron along the c_h -axis further splits the t_{2g} level into a doubly degenerate e^{π} and a non-degenerate a_1 levels with the C_{3v} symmetry. In the corundum structure, the layers of the honeycomb lattice of V ions are stacking along the c_h -axis and each V ion in the layers forms a V ion pair along the c_h -axis with a V ion in the adjacent layer. While the a_1 orbitals point to the direction of the c_h -axis, forming strong σ bonds in the V ion pairs, the e^{π} orbitals extend their lobes toward the direction perpendicular to the c_h -axis, having π bonds with the three neighbors in the layer.

As was first suggested by Allen, here, it is assumed that the electrons are delocalized within the nearest-neighbor V ion pair and interaction between much farther V ions are weak.²²⁾ The two V ions of the pair along the c_h -axis and electron hopping between them were considered based on configuration interaction ap-

proach.^{24–26} In each V ion site, the fivefold 3d orbitals are fully included and the Coulomb and exchange interactions among 3d electrons, the 3d spin-orbit interaction and the trigonal crystal field are considered.²⁷ The Hamiltonian for the V ion pair model then would be written as

$$\begin{aligned}
 H_{\text{elec}} = & \sum_{i,\nu} \varepsilon_d(\nu) n_{i\nu} + \frac{U_{dd}}{2} \sum_{i,\nu,\nu'} n_{i\nu} n_{i\nu'} \\
 & + \sum_{\nu,\nu'} V(\nu, \nu') (a_{A,\nu}^\dagger a_{B,\nu'} + a_{B,\nu}^\dagger a_{A,\nu'}) \\
 & + \sum_{i,\nu_1, \dots, \nu_4} g(\nu_1, \nu_2; \nu_3, \nu_4) a_{i\nu_1}^\dagger a_{i\nu_2}^\dagger a_{i\nu_4} a_{i\nu_3} \\
 & + \zeta_d \sum_{i,\nu,\nu'} \langle \nu | \mathbf{l} \cdot \mathbf{s} | \nu' \rangle a_{i\nu}^\dagger a_{i\nu'} \\
 & + \sum_{i,\nu \neq \nu'} C_i(\nu, \nu') a_{i,\nu}^\dagger a_{i,\nu'}, \tag{1}
 \end{aligned}$$

where the first and second terms are those for the one body energies of the 3d orbitals, the effective Coulomb repulsion energy between the 3d electrons, respectively, the third term represents the electron hopping between two V ion sites A and B in the V ion pair given in terms of the Slater-Koster parameters $dd\sigma$ and $dd\pi$, the forth term is for the multipole interaction between the 3d electrons, which is described by the Slater integrals F_{dd}^2 and F_{dd}^4 of the 3d orbital and the fifth term denotes the 3d spin-orbit interaction with the coupling constant ζ_d . The last term represents crystal field due to the monoclinic lattice distortion in the AFI phase. Here, ν represents the combined index of the species of the 3d orbital and the spin quantum number of the electron, $i = A, B$ stands for the V ion site and $a_{i\nu}^\dagger$ creates an electron on the 3d orbital with ν at the V ion site i .

In a C_{3v} crystal field, the five degenerate 3d orbitals split into one non-degenerate a_1 orbital and two doubly-degenerate e orbitals. Using coordinates where z -axis is parallel to the c_h -axis of the corundum structure and y -axis to one of the three V-V bond direction in the \mathbf{a}_h - \mathbf{b}_h basal plane (see Fig. 1), the wavefunctions for the 3d orbitals in terms of the C_{3v} basis functions are written as

$$\begin{aligned}
 |a_1 : i\rangle &= |3z^2 - r^2\rangle, \\
 |e_u^\pi : i\rangle &= s_i \sqrt{\frac{2}{3}} |x^2 - y^2\rangle - \sqrt{\frac{1}{3}} |zx\rangle, \\
 |e_v^\pi : i\rangle &= -s_i \sqrt{\frac{2}{3}} |xy\rangle - \sqrt{\frac{1}{3}} |yz\rangle, \\
 |e_u^\sigma : i\rangle &= s_i \sqrt{\frac{1}{3}} |x^2 - y^2\rangle + \sqrt{\frac{2}{3}} |zx\rangle, \\
 |e_v^\sigma : i\rangle &= -s_i \sqrt{\frac{1}{3}} |xy\rangle + \sqrt{\frac{2}{3}} |yz\rangle,
 \end{aligned}$$

where the two kinds of e orbitals in the C_{3v} symmetry originating from the t_{2g} (e_g) orbitals in the O_h symmetry is specified by superscript π (σ), the subscripts u and v indicate two different kinds of basis functions in each e symmetry orbitals and s_i takes either $+1$ or -1

depending on the orientation of the oxygen octahedron surrounding the i -th V ion site and has different sign between the two V ions in each V ion pair. The energies of these orbitals $\varepsilon_d(\nu)$ can be expressed in terms of the octahedral Dq and the trigonal D_{trg} crystal fields parameters:

$$\begin{aligned}
 \varepsilon_d(a_1) &= -4Dq + 2D_{\text{trg}}/3, \\
 \varepsilon_d(e_u^\pi) &= \varepsilon_d(e_v^\pi) = -4Dq - D_{\text{trg}}/3, \\
 \varepsilon_d(e_u^\sigma) &= \varepsilon_d(e_v^\sigma) = 6Dq.
 \end{aligned}$$

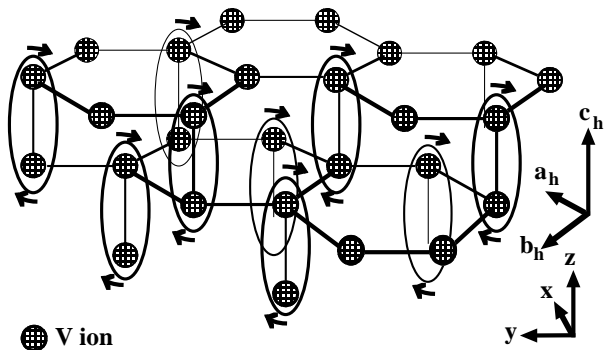


Fig. 2. Schematic drawing of the monoclinic distortion of the V_2O_3 in the AFI phase. The circles denote V ions and the ovals show the V ion pairs. The arrows represent the directions of the tilting of the V-V bond direction in the AFI phase.

In the AFI phase, the crystal structure is distorted from the corundum structure to the monoclinic one. This distortion causes tilting of the V-V bond direction of every V ion pair from the z -axis toward the negative side of the y -axis and breaks three fold rotational symmetry (see Fig. 2). A low symmetry crystal field, which hybridizes the e_v and a_1 orbitals and also the e_v and e_u orbitals on the same site, is present in this phase. Although there are five independent parameters for this low symmetry crystal field $C_i(e_v^\pi, a_1)$, $C_i(e_u^\pi, e_v^\pi)$, $C_i(e_v^\sigma, a_1)$, $C_i(e_v^\sigma, e_u^\sigma)$ and $C_i(e_v^\pi, e_u^\sigma)$, the most important are those related to the e^π orbitals: $C_i(e_v^\pi, a_1)$ and $C_i(e_u^\pi, e_v^\pi)$. Other three parameters involving e^σ orbitals are, for simplicity, all assumed to be zero. Note that there are relations between these parameters for the two V ion sites in the pair: $C_A(e_v^\pi, a_1) = C_B(e_v^\pi, a_1)$, $C_A(e_u^\pi, e_v^\pi) = -C_B(e_u^\pi, e_v^\pi)$.

From recent analysis of high-energy spectroscopy spectra, V_2O_3 is not simply ascribed to the Mott-Hubbard type insulator, where the 3d orbital is the main component of the valence-band top and the conduction-band bottom, but intermediate between the Mott-Hubbard and charge-transfer type insulators, where both the valence-band top and conduction-band bottom consist of highly mixed states of the 3d and O 2p orbitals.^{28–30} It should be emphasized that although the model we assume here does not contain the O 2p orbitals explicitly, the effects of the hybridization between the 3d and 2p orbitals can be partially included by using renormalized param-

eters. As will be discussed next section, the on-site effective Coulomb energy between the $3d$ electrons should be strongly renormalized by this d - p hybridization.

2.2 Effect of d - p hybridization

Before discussing the details of the ground state properties obtained from the model, in this subsection, we will briefly consider the effects of hybridization between the V $3d$ and the nearest neighbor O $2p$ orbitals. To this end, here we compare a single V^{3+} ion model with a VO_6 cluster model,²⁴⁾ in which the V $3d$ orbital and $2p$ orbitals of the six oxygens surrounding the V ion octahedrally are included. The parameters adopted in the cluster model are the effective on-site $3d$ - $3d$ Coulomb energy $U_{dd}=4.0$ eV, the charge transfer energy between the $3d$ and $2p$ orbitals $\Delta=4.0$ eV, the Slater-Koster parameters for the $3d$ - $2p$ hybridization $pd\sigma=-1.73$ eV and $pd\pi=0.75$ eV and the octahedral crystal field $10Dq=1.0$ eV. These parameter values are deduced from the high-energy spectroscopy experiments.²⁸⁾ The configurations $3d^{2+n}\underline{L}^n$ ($n=0, 1, 2, 3$) are assumed for the VO_6^{9-} cluster, where \underline{L} denotes a hole in the O $2p$ orbital. For the Slater integrals of the $3d$ - $3d$ multipole interactions F_{dd}^2 and F_{dd}^4 , the atomic Hartree-Fock values reduced to 80% are used for the VO_6 cluster model.

Table I. Eigen energies relative to the ground state energy for the lowest ten states calculated with the VO_6^{9-} cluster and the V^{3+} ion models are shown. The representation in the O_h symmetry and dominant electron occupation in the $3d^2$ configuration of each eigen state (enclosed by the parentheses) are also listed.

Eigen state	Energy (eV)		
	Cluster	Ion	
3T_1 (t_{2g}^2)	0	0	
1T_2 (t_{2g}^2)	1.40	1.37	
1E (t_{2g}^2)	1.42	1.40	
3T_2 ($t_{2g}e_g$)	1.70	1.53	
3T_1 ($t_{2g}e_g$)	2.68	2.82	
1A_1 (t_{2g}^2)	2.81	2.84	
1T_2 ($t_{2g}e_g$)	3.14	3.10	
1T_1 ($t_{2g}e_g$)	3.39	3.23	
3A_2 (e_g^2)	3.57	3.42	
1E (e_g^2)	4.86	4.77	

In Table I, the lowest ten eigen energies with respect to the ground state energy calculated with the VO_6^{9-} cluster and the single V^{3+} ion models are listed. For simplicity, the $3d$ spin-orbit interaction is not considered in both the models. For the V^{3+} ion model, the Slater integrals $\tilde{F}_{dd}^{2,4}$ reduced to 90% of those for the cluster model and $10\tilde{D}q=1.7$ eV are adopted for the V^{3+} ion model. In the ground state of the VO_6^{9-} cluster model, the weights of the configurations $3d^2$, $3d^3\underline{L}$, $3d^4\underline{L}^2$ and $3d^5\underline{L}^3$ are 41.8%, 44.6%, 12.5% and 1.1%, respectively. Although such strong $3d$ - $2p$ hybridization, it is clearly seen in Table I that the energy level scheme of the VO_6^{9-} cluster is well reproduced by the V^{3+} ion model with the renormalized parameters $\tilde{F}_{dd}^{2,4}$ and $10\tilde{D}q$. Similar low laying level correspondence was found between the VO_6^{10-} cluster and V^{2+} ($3d^1$) ion calculations and also

between the VO_6^{8-} cluster and V^{4+} ($3d^3$) ion calculations. Because of this correspondence of the energy levels of the two, the V ion model would be good starting point to describe the electronic state of V_2O_3 .

The effective on-site Coulomb energy between “ $3d$ electrons” for the V ion model is greatly reduced compared to the model with the O $2p$ orbitals. The on-site effective Coulomb energy between two different “ t_{2g} orbitals” \tilde{U}' can be estimated from the VO_6 cluster model by $\tilde{U}'=E_g(VO_6^{8-})+E_g(VO_6^{10-})-2E_g(VO_6^{9-})$, where E_g 's denote the ground state energies of the clusters with different charges. The on-site Coulomb energy between electrons on the same “ t_{2g} orbital” \tilde{U} and the on-site exchange energy of the “ t_{2g} orbitals” \tilde{J} was obtained by using $\tilde{U}=\tilde{U}'+6\tilde{F}_2+40\tilde{F}_4$ and $\tilde{J}=3\tilde{F}_2+20\tilde{F}_4$.²⁷⁾ The values obtained are $\tilde{U}=3.61$ eV, $\tilde{U}'=2.31$ eV and $\tilde{J}=0.65$ eV. Similarly, the renormalized value for U_{dd} was obtained by $\tilde{U}_{dd}=\tilde{U}'+\frac{4}{9}\tilde{F}_2-10\tilde{F}_4=2.07$ eV. These are the values which should be used in models in which the O $2p$ orbitals are not explicitly included. For comparison, these quantities for the bare t_{2g} orbitals obtained with $U_{dd}=4.0$ eV and $F_{2,4}$ reduced to 80% from Hartree-Fock values are $U=5.60$ eV, $U'=4.15$ eV and $J=0.73$ eV.

Table II. Values of the renormalized parameters adopted in the V ion pair model. For the d - d hopping integrals and the crystal field parameters $C_A(e_v^\pi, a_1)$ and $C_A(e_u^\pi, e_v^\pi)$, values for the AFI and PM phases are indicated. All values are units of eV.

			(AFI)	(PM)
U_{dd}	2.07	$dd\sigma$	-0.735	-0.793
F_{dd}^2	7.29	$dd\pi$	0.100	0.109
F_{dd}^4	4.57	$dd\delta$	0	0
$10Dq$	1.7	$C_A(e_v^\pi, a_1)$	0.02	0
ζ_d	0.023	$C_A(e_u^\pi, e_v^\pi)$	-0.02	0

Because of this strong d - p mixing, the hopping integrals $dd\sigma$, $dd\pi$ and $dd\delta$ between the two V ion sites in the pair must be also renormalized. Effective d - d hopping matrix elements, where the influence of the d - p mixing is considered within the second-order perturbation theory, are

$$\begin{aligned}
 V(a_1, a_1) &\simeq \frac{1}{N_\pi} \left(dd\sigma - \frac{2(pd\pi)^2}{3\Delta} \right), \\
 V(e_\gamma^\pi, e_\gamma^\pi) &\simeq \frac{1}{N_\pi} \left(-\frac{1}{3}dd\pi + \frac{2}{3}dd\delta + \frac{4(pd\pi)^2}{3\Delta} \right), \\
 V(e_\gamma^\sigma, e_\gamma^\sigma) &\simeq \frac{1}{N_\sigma} \left(-\frac{2}{3}dd\pi + \frac{1}{3}dd\delta + \frac{(pd\sigma)^2}{2\Delta} \right), \\
 V(e_\gamma^\sigma, e_\gamma^\pi) &= V(e_\gamma^\pi, e_\gamma^\sigma) \\
 &\simeq \frac{\sqrt{2}}{3\sqrt{N_\pi N_\sigma}} \left(dd\pi + dd\delta - \frac{\sqrt{6}(pd\pi)(pd\sigma)}{\Delta} \right),
 \end{aligned}$$

where $\gamma=u, v$, $N_\pi=1+4(pd\pi)^2/\Delta$ and $N_\sigma=1+6(pd\sigma)^2/\Delta$. Using parameter values for $pd\sigma$, $pd\pi$ and Δ deduced from the high-energy spectroscopy experiments mentioned before, it is found that values of the matrices other than $V(a_1, a_1)$ is largely reduced from those

without d - p hybridization. Such the effects of the d - p hybridization was included approximately by reducing the value of $dd\pi$ to 25% from the bare value. Harrison's values are adopted as for the bare values of the d - d hopping integrals.³¹⁾ The renormalized parameters adopted in the V ion pair model are summarized in Table. II.

2.3 Properties of ground state

In this subsection, we will discuss the ground state

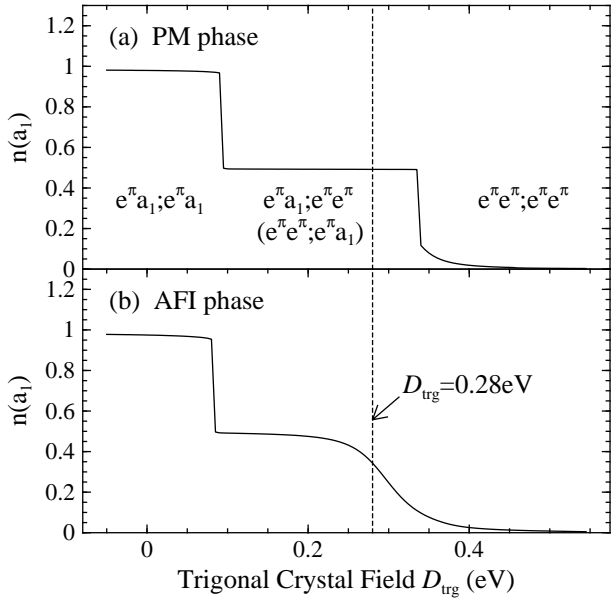


Fig. 3. Trigonal crystal field D_{trg} dependence of the a_1 orbital occupation number per V ion in the ground state for the PM (a) and AFI (b) phases are shown. The vertical line is positioned at $D_{\text{trg}} = 0.28$ eV where the ground state gives the ratio $e^{\pi}a_1 : e^{\pi}e^{\pi} = 1 : 2$ deduced from the XAS experiment for the AFI phase.

properties of the V_2O_3 , using the model described in § 2.1. In Fig. 3(a), the trigonal crystal field D_{trg} dependence of the a_1 orbital occupation number for a V ion in the ground state for the PM phase is shown. Two discontinuous decrease in the occupation number at $D_{\text{trg}} = 0.09$ eV and $D_{\text{trg}} = 0.34$ eV are seen as D_{trg} increases. Because of the Hund's rule coupling, the spins of two electrons in each V ion site form $S = 1$ spin state in the ground state. This is very different result to the model proposed by Castellani *et al.*,¹³⁾ where one electron-spin in the a_1 orbital couples to that of the other V ion of the pair forming a singlet spin state with the neighboring site and $S = 1/2$ spin degree of freedom arising from the other electron in the the e^{π} orbital remains in each V ion site. The difference in the spin state of the V ions is essentially caused by their choice of the on-site exchange interaction value $\tilde{J} \sim 0.2$ eV, which is less than one third of our value. For $D_{\text{trg}} < 0.09$ eV, where energy of the a_1 orbital is lower than that of the e^{π} orbital, one of electrons is in the e^{π} orbital and the other is in the a_1 orbital in both V ion sites (denoted by $e^{\pi}a_1; e^{\pi}a_1$). On

the other hand, for $D_{\text{trg}} > 0.34$ eV, two e^{π} orbital are occupied in both V ion site (denoted by $e^{\pi}e^{\pi}; e^{\pi}e^{\pi}$). In between these two region, the ground state is a superposition of the $e^{\pi}e^{\pi}; e^{\pi}a_1$ and $e^{\pi}a_1; e^{\pi}e^{\pi}$ states.

For $0.09 < D_{\text{trg}} < 0.34$, the ground state is doublet state and their wave functions $|g\pm\rangle$ in large U and $10Dq$ limit can be approximately described by

$$|g+\rangle = \frac{1}{\sqrt{2}}(|e_{+1}^{\pi}a_1; e_{+1}^{\pi}e_{-1}^{\pi}\rangle + |e_{+1}^{\pi}e_{-1}^{\pi}; e_{+1}^{\pi}a_1\rangle),$$

$$|g-\rangle = \frac{-1}{\sqrt{2}}(|e_{-1}^{\pi}a_1; e_{+1}^{\pi}e_{-1}^{\pi}\rangle + |e_{+1}^{\pi}e_{-1}^{\pi}; e_{-1}^{\pi}a_1\rangle),$$

where \uparrow (\downarrow) denotes the magnetic quantum number of the electron spin $s_z = 1/2$ ($s_z = -1/2$) and $|e_{\pm}^{\pi}\rangle = \frac{1}{\sqrt{2}}(\mp|e_u^{\pi}\rangle - i|e_v^{\pi}\rangle)$ with $\langle e_{\pm}^{\pi}|L_z|e_{\pm}^{\pi}\rangle = \mp 1$. These states have the orbital and spin angular momenta along the z -axis and the values per V ion are $\langle g\pm|L_z|g\pm\rangle = \mp \frac{1}{2}$ and $\langle g\pm|S_z|g\pm\rangle = \pm 1$. Since this degeneracy of ground state is magnetic, there is no orbital degree of freedom. This is very different result to the similar V ion pair model propose by Mila *et al.*,^{18,19)} where the orbital angular momentum is assumed to be small and thus the orbital degree of freedom still remains apart from the spin degree of freedom. The ground state wave functions of their model are written as

$$|g\gamma; S_z^{\text{T}}\rangle = \frac{1}{\sqrt{2}}(|e_{\gamma}^{\pi}a_1; e_u^{\pi}e_v^{\pi}\rangle + |e_u^{\pi}e_v^{\pi}; e_{\gamma}^{\pi}a_1\rangle) \otimes |S^{\text{T}} = 2; S_z^{\text{T}}\rangle,$$

where γ specifies the two kinds of the e^{π} orbitals u and v and $|S^{\text{T}} = 2; S_z^{\text{T}}\rangle$ is the total-spin wavefunction, in which $S = 1$ Hund's spins of the two V ions are coupled ferromagnetically. The ground state wavefunctions of our model $|g\pm\rangle$ can be describe in terms of the wavefunctions $|g\gamma; S_z^{\text{T}}\rangle$ as

$$|g\pm\rangle = \frac{1}{\sqrt{2}}(-i|gu; S_z^{\text{T}} = \pm 2\rangle \pm |gv; S_z^{\text{T}} = \pm 2\rangle). \quad (2)$$

The wavefunctions of Mila's ground state other than above two are lifted higher energies ranging upto ~ 0.027 eV.

It has been reported from the x-ray diffraction experiment that the distortion from the corundum structure to the monoclinic structure at the PM \rightarrow AFI transition involves abrupt expansion of the V-V bond length of the V ion pair and rotation of the V-V bond direction about 1.8° from the c_h -axis (within the y - z plane in Fig. 2).²⁾ To take into account the effects of the lattice distortion, the values of $dd\sigma$ and $dd\pi$ are reduced from those for the PM phase using the V-V distance R dependence ($ddm \propto 1/R^5$ proposed by Harrison³¹⁾ and the low symmetry crystal field are considered as in Table II.

In Fig. 3(b), the trigonal field D_{trg} dependence of the a_1 orbital occupation number in the ground state for the AFI phase is shown. The most different part compared to Fig. 3(a) is that the occupation number decreases continuously as D_{trg} increases around $D_{\text{trg}} \sim 0.3$ eV. This indicates that the boundary between the $e^{\pi}e^{\pi}; e^{\pi}e^{\pi}$ and $e^{\pi}a_1; e^{\pi}e^{\pi}$ ($e^{\pi}e^{\pi}; e^{\pi}a_1$) states is obscure and around $D_{\text{trg}} \sim 0.3$ eV, there is $e^{\pi}e^{\pi}; e^{\pi}e^{\pi}$ and $e^{\pi}a_1; e^{\pi}e^{\pi}$ ($e^{\pi}e^{\pi}; e^{\pi}a_1$) mixed state. This can be understood as follows. Because of the symmetry lowering of the pair caused by the tilting of the V-V bond direction from the trigonal axis,

the a_1 and e_v^π orbitals hybridized in each other. This leads to hybridization of the $e^\pi e^\pi; e^\pi e^\pi$ and $e^\pi a_1; e^\pi e^\pi$ ($e^\pi e^\pi; e^\pi a_1$) states around $D_{\text{trg}} \sim 0.3$ eV, where energies of these two states are almost degenerate. It is also seen in Fig. 3(b), the boundary is shifted to much lower D_{trg} than that for the PM phase. This shift of the boundary is due to reduction in the V-V hopping integral values.

If we assume $D_{\text{trg}} \sim 0.3$ eV, the abrupt change in the a_1 orbital occupation number is expected at the metal-insulator (M-I) transition. Such a large difference in the a_1 orbital occupation number between the metal and insulating phases was indeed inferred from the measurement of the linear dichroism of the V 2p X-ray absorption spectrum.¹⁴⁾ Both the $e^\pi a_1$ to $e^\pi e^\pi$ ratio estimated from the measurement for the AFI phase $e^\pi a_1 : e^\pi e^\pi = 1 : 2$ and the PM phase $e^\pi a_1 : e^\pi e^\pi = 1 : 1$ are well reproduced with $D_{\text{trg}} = 0.28$ eV. Since large change in the electronic state are caused by the lattice distortion, i.e., elongation and rotation of the V-V bond of the V ion pair, in this model, it is expected that the lattice distortion is strongly related to the metal-insulator transition. It is also important to mention that there is also large difference in the weight of the d^3d^1 and d^1d^3 configurations between the ground states obtained for the two phases. While the weight is $w(d^3d^1) = w(d^1d^3) = 3.5\%$ for the AFI phase, the weight for the PM phase is 6.9%. Such large increase of the charge fluctuation from the AFI phase to the PM phase in this model again indicates strong connection between the monoclinic distortion and this metal-insulator transition.

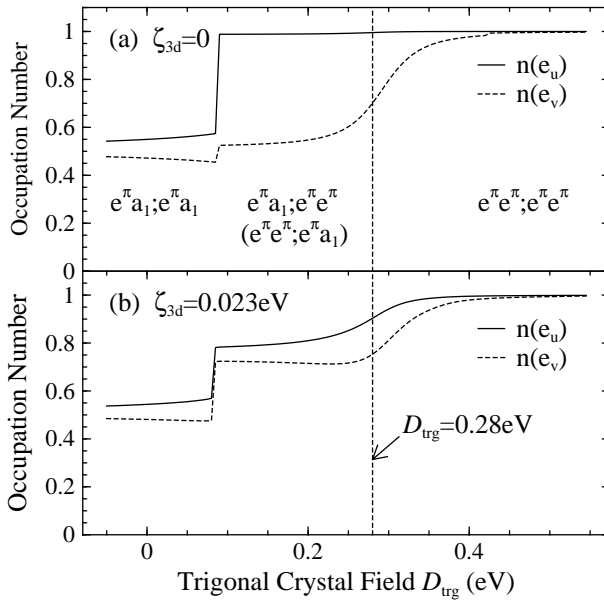


Fig. 4. Trigonal crystal field D_{trg} dependence of the e_u (e_v) orbital occupation number $n(e_u)$ ($n(e_v)$) per V ion in the ground state without (a) and with (b) the 3d spin-orbit interaction for the AFI phase are shown. The vertical line is positioned at $D_{\text{trg}} = 0.28$ eV, where the ground state gives the ratio $e^\pi a_1 : e^\pi e^\pi = 1 : 2$ deduced from the XAS experiments for the AFI phase.

To see the effects of the 3d spin-orbit interaction on the ground state wavefunction in the AFI phase much clearly, in Fig. 4, D_{trg} dependence of the e_u and e_v orbital occupation numbers $n(e_u)$ and $n(e_v)$ per V ion without (a) and with (b) the 3d spin-orbit interaction are shown for the AFI phase. There is large difference between the two cases. For $0.09 < D_{\text{trg}} < 0.25$, without the spin-orbit interaction, the occupation numbers are $n(e_u) \sim 1$ and $n(e_v) \sim 1/2$ and this shows that the ground state is mainly dominated by the $e_u^\pi a_1; e_u^\pi e_v^\pi$ ($e_u^\pi e_v^\pi; e_u^\pi a_1$) configuration. This also indicates that the monoclinic distortion will induce the ferro V₂ molecular orbital order in the AFI phase, which is proposed by Mila *et al.*^{18,19)} On the other hand, in the same parameter range, with the spin-orbit interaction, the occupation numbers are $n(e_u) \sim n(e_v) \sim 3/4$ and both two kinds of the configurations $e_u^\pi a_1; e_u^\pi e_v^\pi$ and $e_v^\pi a_1; e_v^\pi e_u^\pi$ are almost in equal weight. As was discuss before, this is because the strong coupling between the spin and orbital degeneracy and there are no orbital degree of freedom which is independent to the spin degree of freedom in this ground state and thus we do not expect usual Jahn-Teller instability. Around $D_{\text{trg}} \sim 0.3$ eV, where the $e^\pi e^\pi; e^\pi e^\pi$ state are mixed with the $e^\pi a_1; e^\pi e^\pi$ ($e^\pi e^\pi; e^\pi a_1$) state, the situation is similar: difference between $n(e_u)$ and $n(e_v)$ are smaller with the spin-orbit interaction than that without the interaction.

The ground state property with the spin-orbit interaction above can be understood more clearly with the aide of an effective Hamiltonian within the limit of large U and $10Dq$. In this limit, the ground state is well described within restricted basis functions $|ge\rangle = |e_u^\pi e_v^\pi; e_u^\pi e_v^\pi\rangle$ and $|g\gamma\rangle = \frac{1}{\sqrt{2}}(|e_\gamma^\pi a_1; e_u^\pi e_v^\pi\rangle + |e_u^\pi e_v^\pi; e_\gamma^\pi a_1\rangle)$ ($\gamma = u, v$). For convenience, here, $L' = 1$ pseudo orbital angular momentum operator \mathbf{L}' is introduced, where the eigen functions $L'_z|g\ m\rangle = m|g\ m\rangle$ of L'_z are defined by $|g\ m = 0\rangle = -|ge\rangle$ and $|g\ m = \pm 1\rangle = (-i|gu\rangle \pm |gv\rangle)/\sqrt{2}$. The effective Hamiltonian can be expressed using \mathbf{L}' and the $S^T = 2$ total spin operator \mathbf{S}^T of the V ion pair as

$$H_{\text{eff}} = -\lambda \{ S_z^T L'_z + \sqrt{2}(S_x^T L'_x + S_y^T L'_y) \} + \Delta L'_z + \sqrt{2}C_A(e_v^\pi, a_1)(L'_z L'_y + L'_y L'_z), \quad (3)$$

where $\lambda = \zeta_{3d}/4$ and $\Delta = D_{\text{trg}} - \{(dd\sigma)^2 + (dd\pi/3)^2\}/(U' - J)$. Note that there are relations between the real total orbital angular momentum operator \mathbf{L} and \mathbf{L}' within this restricted basis: $L_x = -\sqrt{2}L'_x$, $L_y = -\sqrt{2}L'_y$ and $L_z = -L'_z$. If $C_A(e_v^\pi, a_1) = 0$, the system has uniaxial anisotropy and when $\Delta < -2\lambda$, the z -axis is the magnetic easy axis and the ground state is $|g\pm\rangle = |g\ m = \pm 1\rangle |S_z^T = \pm 2\rangle$, which is identical to that in eq. (2). On the other hand, for $\Delta > -2\lambda$, the x - y plane is the magnetic easy plane. With finite $C_A(e_v^\pi, a_1)$, the term $(L'_z L'_y + L'_y L'_z)$ causes hybridization between $|ge\rangle$ and $|gu\rangle$ and this rotate the magnetic easy axis from the z -axis toward the y -axis. The ground state can be regarded as magnetic doublet state having their magnetic moments along this easy axis with opposite directions in each other, although breaking of the rotational symmetry around this easy axis causes a small energy splitting < 0.5 meV between these lowest two eigen states.

2.4 Magnetic anisotropy

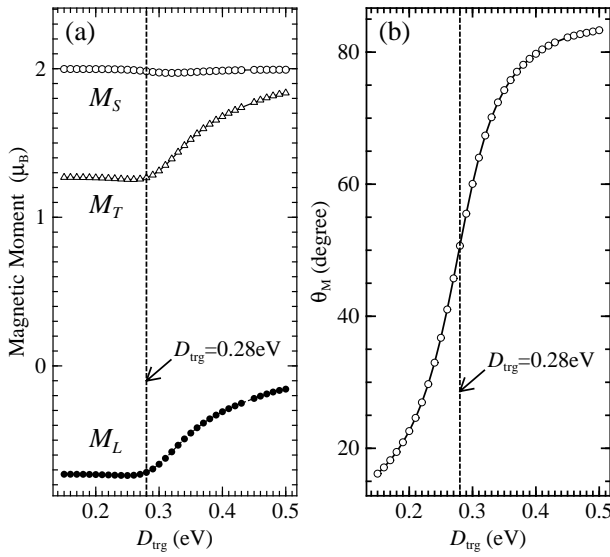


Fig. 5. Sizes of the spin M_S , orbital M_L and total M_T magnetic moments (a) and the canting angle of the total magnetic moment from the z -axis θ_M (b). as a function of the trigonal crystal field D_{trg} .

As was discussed in the previous subsection the admixture of the $e^\pi e^\pi; e^\pi e^\pi$ state in the ground state lead to rotation of the magnetic easy axis. To study such magnetic properties of the ground state, a molecular field H_M with a canting angle θ_M with respect to the z -axis in the y - z plane was further applied in the V ion pair model:

$$H_{\text{mol}} = H_M \sum_{\gamma} \{ \cos \theta_M (a_{A\gamma\uparrow}^\dagger a_{A\gamma\uparrow} - a_{A\gamma\downarrow}^\dagger a_{A\gamma\downarrow}) - i \sin \theta_M (a_{A\gamma\uparrow}^\dagger a_{A\gamma\downarrow} - a_{A\gamma\downarrow}^\dagger a_{A\gamma\uparrow}) \}.$$

In the calculation, the molecular field with the magnitude $H_M = 0.01$ eV is adopted and θ_M was chosen so as to give the lowest ground state energy. The magnetic moment is, therefore, parallel to both the magnetic easy axis and the molecular field. Note that the values and direction of the spin and orbital magnetic moments obtained here are not sensitive to the magnitude of the molecular field.

In Fig. 5, the sizes of the spin M_S , orbital M_L and total M_T magnetic moments per V ion (a) and θ_M (b) are shown as a function of D_{trg} . Both the directions of the magnetic moment and the V ion pair are in the y - z plane. For the $e^\pi a_1; e^\pi e^\pi$ ($e^\pi e^\pi; e^\pi a_1$) ground state, the direction of the magnetic moment is parallel to the z -axis (the corundum c_h -axis). However, as the weight of the $e^\pi e^\pi; e^\pi e^\pi$ configuration in the ground state increases, the magnetic moment is canted toward the y -axis and finally reaches to the y -axis with a pure $e^\pi e^\pi; e^\pi e^\pi$ ground state. Note that the V-V bond of the V ion pair is tilted toward opposite direction to the magnetic moment, i.e., toward the negative direction of the y -axis. The large

orbital magnetic moment $M_L \sim 0.7\mu_B$ is present in the $e^\pi a_1; e^\pi e^\pi$ ($e^\pi e^\pi; e^\pi a_1$) ground state. The orbital magnetic moment is about 40% larger than that expected from the ground state wavefunction (see eq. (2)) in the limit of large U and $10Dq$. This deviation is mainly due to the presence of the small weight of configurations with occupied e^σ orbitals arising from the 3d-3d multipole interaction. While M_S remains almost unchanged $M_S \sim 2\mu_B$ as the weight of the $e^\pi e^\pi; e^\pi e^\pi$ configuration increases, M_L decreases rapidly. At $D_{\text{trg}} = 0.28$ eV, $M_T \sim 1.2\mu_B$ and $\theta_M = 51^\circ$ and these well agree with the values obtained in the neutron diffraction experiments $M_T \sim 1.2\mu_B$ and $\theta_M \sim 71^\circ$.⁸⁾ Strictly speaking, the magnetic moments of the two V ions are slightly tipped out from the y - z plane toward opposite direction in each other. Although the x-component of the magnetic moments is an order of $\sim 0.01\mu_B$, the fact is important for the interpretation of the RXS measurements as will be discussed in § 5.3.

§3. Electron-Lattice Interaction

As was discussed in § 2.3, the pure $e^\pi a_1; e^\pi e^\pi$ ($e^\pi e^\pi; e^\pi a_1$)

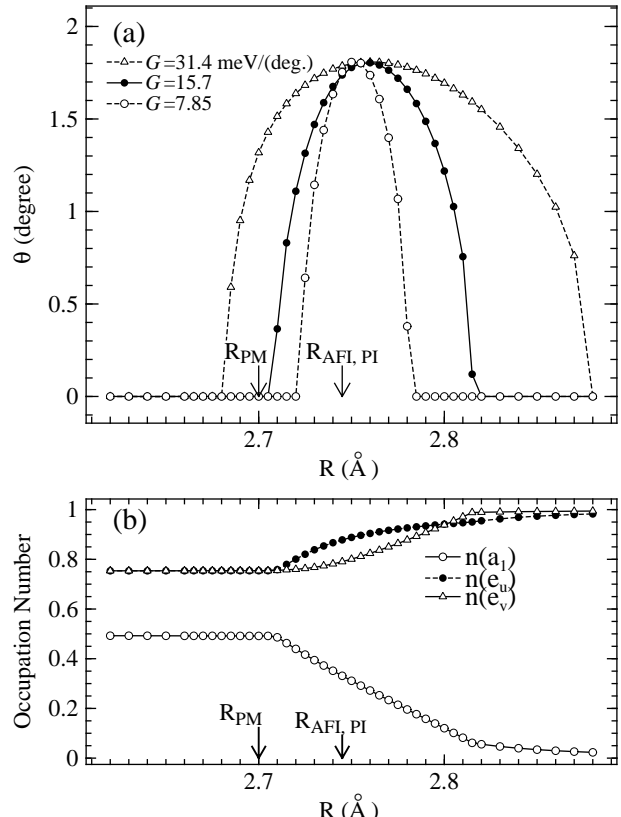


Fig. 6. In (a), tilting angle from the c_h -axis as a function of the V-V distance of the V ion pair R is shown for $G = 7.85, 15.7$ and 31.4 meV/(°). $R_{\text{AFI, PI}}$ denote the experimentally observed V-V distance of the V ion pair in both the AFI and PI phases whereas R_{PM} shows that in the PM phase. In (b), the a_1 , e_u and e_v orbital occupation numbers calculated with $G = 15.7$ meV/(°) are shown.

ground state has only spin degree of freedom and no or-

bial degree of freedom is left behind. One would not, therefore, expect usual Jahn-Teller lattice instability in this system. However, in the AFI phase, V_2O_3 exhibits the monoclinic lattice distortion and this indicates that there must be some other kind of lattice instability in this system. Here, it will be shown that such instability indeed appears when the energy of the $e^\pi a_1; e^\pi e^\pi$ ($e^\pi e^\pi; e^\pi a_1$) and $e^\pi e^\pi; e^\pi e^\pi$ states are almost degenerate.

In order to discuss interaction between the lattice deformation and the electronic state, here, we consider one V ion pair in the crystal and in addition to the energy of the electronic state discussed in § 2.1, the local lattice deformation energy caused by tilting of the V ion pair is included. The energy of the V ion pair as a function of the polar θ and azimuthal φ angles of the tilting direction would be written in the form:

$$E_{\text{tot}}(\theta, \varphi) = E_{\text{elec}}(\theta, \varphi) + \frac{K}{2}\theta^2 + F\theta^3 \sin 3\varphi + \dots, \quad (4)$$

where the first term denotes the ground state energy of the Hamiltonian described in § 2.1 and the second and third terms are the local lattice distortion energies.

Instead of including $F\theta^3 \sin 3\varphi$ and much higher order trigonal potential terms of the lattice deformation, for simplicity, we consider the lowest term $\frac{K}{2}\theta^2$ only and assume that tilting occurs only to the restrict directions of $\varphi = -\frac{\pi}{2}, -\frac{\pi}{2} \pm \frac{2\pi}{3}$, where displacements of each V ion of the pair is parallel to one of the three V-V bond in the honeycomb layer. As a result, the V-V bond along this direction is elongated and those in the other two directions contract. Note that this tilting direction is consistent with that observed in the monoclinic lattice distortion in the AFI phase. In such lattice distortion, both the e_u^π and e_v^π orbitals can be hybridized with the a_1 orbital and corresponding low symmetry crystal field parameters, which are linear functions in θ for small lattice distortion, can be written in the form:

$$C_A(e_u^\pi, a_1) = \frac{G\theta}{\sqrt{2}} \cos \varphi, \quad C_A(e_v^\pi, a_1) = \frac{G\theta}{\sqrt{2}} \sin \varphi. \quad (5)$$

In the calculation, $D_{\text{trg}} = 2.8$ eV was adopted and the V-V distance R dependence for the d - d hopping integrals $dd\sigma, dd\pi \propto 1/R^5$ was assumed.

In Fig. 6, the tilting angle at the minimum of E_{tot} as a function of the V-V distance of the V ion pair R is shown for three different crystal fields $G = 7.85$ (open circles), 15.7 (closed circles) and 31.4 meV/($^\circ$) (triangles). The coefficient K was chosen so that maximum tilting angle is 1.8° and those for $G = 7.85, 15.7$ and 31.4 meV/($^\circ$) are $K = 2.60, 6.50$ and 15.7 meV/($^\circ$)², respectively. The V-V distances $R_{\text{AFI,PI}}$ and R_{PM} are the experimentally observed values in the insulating phases and in the PM phase, respectively.²⁾ The rotation of the V ion pair occurs only when the energy of the two kinds of the states $e^\pi a_1; e^\pi e^\pi$ ($e^\pi e^\pi; e^\pi a_1$) and $e^\pi e^\pi; e^\pi e^\pi$ are nearly degenerate and takes the maximum value around $R = 2.750$ \AA , where the two kinds of the states are just degenerate. Note that the energy difference between the two can be given by $\sim D_{\text{trg}} - \{(dd\sigma)^2 + (dd\pi/3)^2\}/(U' - J)$.

This instability toward the lattice distortion can be

explained by the similar mechanism to the Jahn-Teller effects. If we include the lattice distortion energy, the effective Hamiltonian eq. (3) generalized for the V ion pair with an arbitrary tilting angle (θ, φ) can be written as

$$\begin{aligned} H_{\text{eff}} = & -\lambda \{S_z^T L'_z + \sqrt{2}(S_x^T L'_x + S_y^T L'_y)\} + \Delta L_z'^2 \\ & + G\theta \{\cos \varphi (L'_z L'_x + L'_x L'_z) + \sin \varphi (L'_z L'_y + L'_y L'_z)\} \\ & + \frac{K}{2}\theta^2 + F\theta^3 \sin 3\varphi + \dots \end{aligned} \quad (6)$$

When the energies of the these two kind of states $|ge\rangle$ and $|g\gamma\rangle$ ($\gamma = u, v$) are degenerate or nearly degenerate, the term linear in θ , which couples the states $|ge\rangle$ and $|g\gamma\rangle$, causes rotation of the V ion pair in the same way as the Jahn-Teller effects. The condition for instability toward tilting is approximately obtained for small λ and $|F|$ as $|\Delta| < 2G^2/K$.

Since the energy gain from this electron-lattice interaction is maximum at the V-V distance where the energies of the two kinds of the states are nearly degenerate, if this mechanism is the cause of the monoclinic distortion in the AFI phase, the V-V distance of the pair in this phase should be at this distance. Indeed, the value $R = 2.755$ \AA giving the maximum tilting angle is very near to the value $R_{\text{AFI,PI}} = 2.745$ \AA , where the V 2p XAS experimental results on the $e^\pi e^\pi$ and $e^\pi a_1$ configuration ratio for the AFI phase $e^\pi a_1 : e^\pi e^\pi = 1 : 2$ is reproduced.¹⁴⁾ The monoclinic lattice distortion in the AFI phase thus can be understood by this mechanism. On the other hand, the V-V distance is much shorter in the PM phase $R_{\text{PM}} \sim 2.700$ \AA and if $|G| < 16$ meV, the lattice instability does not occur at this distance. In this situation, pure $e^\pi a_1; e^\pi e^\pi$ ($e^\pi e^\pi; e^\pi a_1$) state is expected in this phase. This also agrees with the V 2p XAS experiment, where $e^\pi a_1 : e^\pi e^\pi = 1 : 1$ is obtained in the PM phase.

Although the experimentally observed V-V distance is the same to that for the AFI phase, in the PI phase, no monoclinic lattice distortion have been found. This can be explain as follows. In the PI phase, each V ion pair is also tilted from the c_h axis similar to the AFI phase. However, their tilting directions are disordered and fluctuate among the three stable directions $\varphi = -\frac{\pi}{2}, -\frac{\pi}{2} \pm \frac{2\pi}{3}$, resulting in no monoclinic lattice distortion. This assumption is consistent with the V 2p XAS experimental results, where weight of the $e^\pi e^\pi$ configuration is larger than that of the $e^\pi a_1$ configuration both in the PI and AFI phases in their initial state, indicating admixture of the $e^\pi e^\pi, e^\pi e^\pi$ configuration. If this assumption is correct, the AFI \rightarrow PI transition is accompanied by order to disorder transition in the tilting directions of the V ion pairs. As will be discussed in the next section, this ordering of the tilting direction in the AFI phase can be explained by a model in which this local lattice distortion and the magnetic exchange interaction between the V ion pairs are considered.

From above discussion, it is expected that there are at least two local minima for the free energy of the real system as a function of the V-V distance of the pair.

One is positioned at $R_{\text{PM}} \sim 2.700 \text{ \AA}$, where the energy difference of the two kinds of the state $e^\pi a_1; e^\pi e^\pi$ and $e^\pi e^\pi; e^\pi e^\pi$ is large and thus no electron-lattice coupling takes place, and the other one is located at $R_{\text{AFI,PI}} \sim 2.745 \text{ \AA}$, where energy of the two kinds of the states is degenerate and Jahn-Teller like lattice distortion is the cause of the energy lowering at this V-V distance. The expansion of the V-V distance in the AFI and PI phases as compared to that in the PM phase can be understood as a consequence of the large change in the $3d$ orbital occupation owing to the tilting of the V ion pair. Since mixture of the $e^\pi e^\pi; e^\pi e^\pi$ state in the ground state reduces electron occupation of the a_1 orbital, which point toward the direction of the V-V bond, the nuclear charges of the V ions of the pair is much less screened by the $3d$ electron in the V-V bond direction, resulting in elongation of the V-V bond.

Since both in the AFI and PI phases, the electron-lattice coupling strongly influences the orbital occupation and charge fluctuation, the $\text{PM} \rightarrow \text{AFI}$ and $\text{PM} \rightarrow \text{PI}$ transitions can not be regarded as usual Mott transition. In § 2.3, it is found that when the lattice distortion occurs, charge fluctuation between the two V ions is strongly suppressed. The expansion of the V-V distance and resultant reduction of the $d-d$ hybridization strength due to this electron-lattice coupling in the insulating phases is probably the main cause of this metal-insulator transition.

§4. Magnetic Interaction between V Ion Pairs

In the previous section, we have discussed about the local lattice distortion effects on the electronic states within individual V ion pairs. Here, we will consider about the exchange interaction between the V ion pairs in its relation with the local lattice distortion in order to discuss the $\text{AFI} \rightarrow \text{PI}$ transition observed in $\text{V}_{1-x}\text{Cr}_x\text{O}_3$. The transition is accompanied by the monoclinic to corundum lattice structure transition and in the ultrasonic wave velocities measurements, the C_{44} elastic constant was estimated to soften almost at the transition temperature, showing the nearly second order nature of the transition.^{11, 12)} Contrary to this, in the AFI to PM transition such softening of C_{44} is not observed and the transition is of the first order. In the magnetic thermal-neutron scattering experiments, abrupt change in short range spin correlation function at the transition temperature was observed.^{9, 10)}

In the AFI phase, the monoclinic lattice distortion and the magnetism are connected, forming unique AF magnetic order. In the monoclinic distortion, all the V ion pairs, which is parallel to the c_h -axis in the corundum structure are tilted $\sim 1.8^\circ$ in the same direction.²⁾ With this displacement of the V ions, the honeycomb lattice, which has three fold rotational symmetry in the corundum structure, is distorted and V-V bonds in one of the three directions in the layer are elongated and those in the other two directions contract (see Fig. 2). The magnetic moments between two V ions with the elongated V-V bond on the honeycomb lattice are ferromagnetically coupled and those with the contracting V-V bond

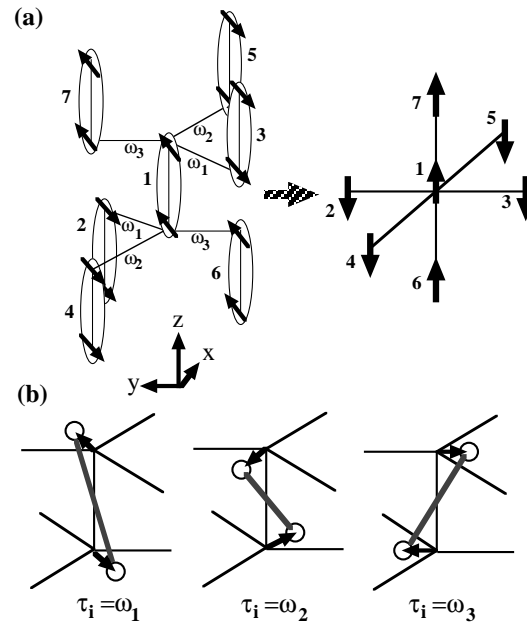


Fig. 7. Mapping of V ion pairs in the corundum lattice on the simple cubic lattice (a) and three possible directions corresponding to $\tau_i = \omega_1, \omega_2$ and ω_3 of the tilting of the V ion pair from the c_h -axis (b) are drawn. On left hand side of Fig. (a), the ovals show the V ion pairs and the arrows represent the spin directions of the V ions and on right hand side, the directions of the pseudo spin $\sigma_i = \pm 1$ for V ion pairs are indicated by the arrows. In Fig. (b), the circles and arrows represent the V ions and their displacement due to the tilting of the V ion pair, respectively.

are antiferromagnetically coupled.

In the theories proposed by Castellani *et al.*¹³⁾ and Mila *et al.*,^{18, 19)} the orbital ordering is an essential ingredient for the formation of this unique AF magnetic order in V_2O_3 , where exchange coupling constant between the spins of V ions depends on the orbital occupation of the V ions. Rice has pointed out that the abrupt change in the spin correlations at the $\text{AFI} \rightarrow \text{PI}$ transition and the short-range spin fluctuations in the PI phase can be explained in the presence of the orbital degree of freedom.³²⁾ Contrary to this, Ezhov *et al.*¹⁷⁾ performed LDA+ U band structure calculations and obtained a solution with the unique AF magnetic order as the lowest total energy magnetic state, assuming the monoclinic lattice distortion. Since the orbital occupation in each V ion is $e^\pi e^\pi$, there are no orbital order in this AF magnetic state. In the present theory, since strong coupling between the spin and orbital degrees of freedom due to the spin-orbit interaction, orbital order does not exist in the ground state. Here, it is assumed that the coupling constant of the exchange interaction is a function of the V-V bond length and not depends on the orbital occupation of the V ions.

4.1 Effective spin-lattice Hamiltonian

The effective spin Hamiltonian considered here consists of the exchange interaction between the nearest

neighbors of the V ion pairs and the local lattice distortion energy in each V ion pair. Each V ion pair has six nearest neighbors and as depicted in Fig. 7, the network of the V ion pairs can be mapped onto the simple cubic lattice. Two spin directions of the doublet ground state on the i -th V ion pair is projected onto Ising like pseudo-spin with $\sigma_i = \pm 1$ at the corresponding lattice point i of this simple cubic lattice. The coupling constant of the exchange interaction is assumed to be a function of the displacement of the V-V bond length due to tilting of the V ion pairs. The effective spin Hamiltonian then can be written as

$$H_S = -J \sum_{\langle i,j \rangle} \{(\theta_i \boldsymbol{\tau}_i + \theta_j \boldsymbol{\tau}_j) \cdot \mathbf{l}_{ij} - C\} \sigma_i \sigma_j + \sum_i \left(\frac{K}{2} \theta_i^2 - G \theta_i \right),$$

where the first term represents the exchange interaction between the pseudo-spins of the V ion pairs and the second term describes the local lattice distortion energy in each V ion pairs. $\theta_i \geq 0$ represents tilting angle of the i -th V ion pair and two dimensional unit vector $\boldsymbol{\tau}_i$ denotes the direction of the tilting projected on the honeycomb layer. Here, we assume that each V ion pair is tilted in such a direction that each V ion in both end is parallel to one of the three V-V bond in the honeycomb layer and elongates this V-V bond. $\boldsymbol{\tau}_i$ is, therefore, in one of these three directions: $\boldsymbol{\omega}_1 = (\sqrt{3}/2, 1/2)$, $\boldsymbol{\omega}_2 = (-\sqrt{3}/2, 1/2)$ or $\boldsymbol{\omega}_3 = (0, -1)$. $\mathbf{l}_{ij} = \boldsymbol{\omega}_1, \boldsymbol{\omega}_2$ or $\boldsymbol{\omega}_3$ indicates the direction of the V-V bond between the i - and j -th V ion pairs. Thus, the term $(\theta_i \boldsymbol{\tau}_i + \theta_j \boldsymbol{\tau}_j) \cdot \mathbf{l}_{ij}$ is proportional to the elongation of the V-V distance between the i - and j -th V ion pairs.

The AF magnetic order observed in V_2O_3 corresponds to the C-type AF magnetic order in this model, where nearest neighbor spins along one of the lattice line in the simple cubic lattice are coupled ferromagnetically and those along the other two are antiferromagnetically coupled (see Fig. 7 (a)). For this AF magnetic order, the energy per V ion pair is easily obtained as a function of a uniform distortion $\theta = \theta_i$

$$E(\theta) = -|J|C - (G + 4|J|)\theta + \frac{K}{2}\theta^2$$

and the energy has minimum at $\theta_{\min} = \frac{G+4|J|}{K}$

$$E(\theta_{\min}) = -|J|C - \frac{1}{2} \frac{(G+4|J|)^2}{K}.$$

For this AF magnetic state being stable, the exchange coupling constant $J(2\theta_{\min} - C)$ for the long V-V length should be positive and that for the short V-V length $-J(\theta_{\min} + C)$ should be negative. Thus at least the conditions $J < 0$ and $2\theta_{\min} > C > -\theta_{\min}$ must be satisfied for this AF magnetic state being the ground state.

4.2 AFI to PI phase transition

To study finite temperature properties of this effective Hamiltonian, Monte Carlo simulations were performed with a $24 \times 24 \times 24$ periodic lattice for various values of C . Figure 8 shows the phase diagram as a function of C and $k_B T / |J|$ obtained from the calculation. The adopted value of G is $G = 15.7 \text{ meV}/(\text{deg.})$ and from the ex-

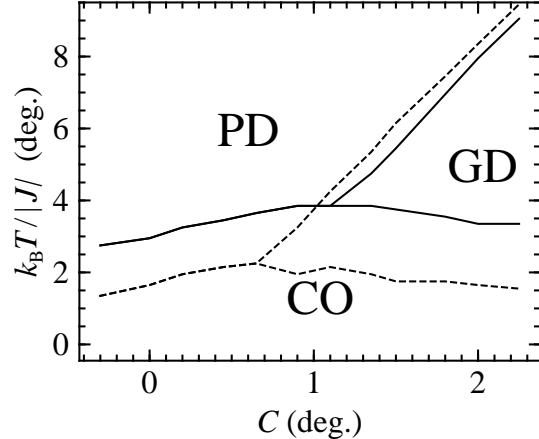


Fig. 8. Phase diagram of the effective spin Hamiltonian for $G/|J| = 3$ (solid line) and $G/|J| = 0$ (dashed line). CO denotes the C-type AF magnetic order with ordered tilting direction of V ion pair. GD and PD are the G-type AF magnetic order and paramagnetic order with disordered tilting direction, respectively.

perimental facts $\theta_{\min} \sim 1.8^\circ$ and $T_N \sim 155 \text{ K}$, the other parameter values are estimated to be $J \sim -4.0 \text{ meV}/(\text{deg.})$, $K/|J| \sim 3.9 \text{ } (\text{deg.})^{-1}$ and $G/|J| \sim 3.0$. The solid and dashed lines represent the phase boundaries calculated with $(G/|J| = 3)$ and without $(G/|J| = 0)$ the electron-lattice coupling, respectively. In the range of $-0.3^\circ < C < 2.25^\circ$ as shown in the figure, the low temperature phase is that with the C-type AF magnetic order and the V ion pairs are tilted and ordered in the same direction in this phase (denoted by CO). This phase corresponds to the AFI phase in the real material. The high temperature phase is paramagnetic and the tilting direction of the V ion pairs are disordered (denoted by PD) and this phase corresponds to the PI phase in the real material. For $C > 1.1^\circ$, there is an intermediate temperature phase with the G-type AF magnetic order, where all the nearest neighbor spins are antiferromagnetically coupled, with disordered tilting directions of the V ion pairs (denoted by GD). The transition from the CO phase to the PD phase is of the second order whereas the CO \rightarrow GD and GD \rightarrow PD phase transitions are of the first order. It is also seen in the figure that the CO phase is further stabilized with the electron-lattice interaction (solid line) than without it (dashed line), showing importance of the interaction for the formation of the C-type AF magnetic order.

In Fig. 9, the order parameter of the tilting of V ion pairs $\langle \theta_i \boldsymbol{\tau}_i \cdot \boldsymbol{\omega}_{\text{ord}} \rangle$ and the tilting angle $\langle \theta_i \rangle$ as a function of temperature are shown for $C = 0.9^\circ$ (solid line) and $C = 1.8^\circ$ (dashed line), where $\boldsymbol{\omega}_{\text{ord}}$ is one of the three possible tilting directions $\boldsymbol{\omega}_l$ ($l = 1, 2, 3$) in which the V ion pairs are ordered. It is seen in the figure that the CO \rightarrow PD transition is of the second order and the CO \rightarrow GD transition is of the first order. The tilting angle $\langle \theta_i \rangle$ in

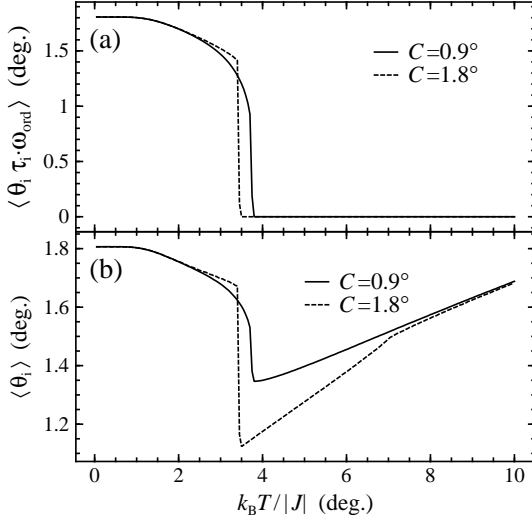


Fig. 9. Order parameter for the tilting of the V ion pairs $\langle \theta_i \tau_i \cdot \omega_{\text{ord}} \rangle$ and the tilting angle $\langle \theta_i \rangle$ as a function of temperature calculated with $C = 0.9^\circ$ (solid line) and $C = 1.8^\circ$ (dashed line).

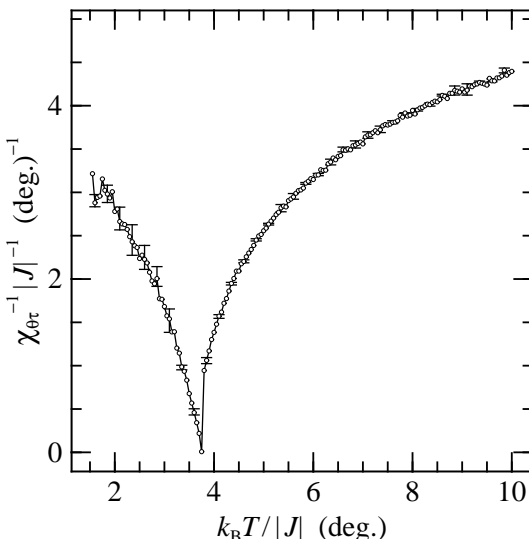


Fig. 10. $1/\chi_{\theta\tau}(T)$ is plotted with error bars for $C = 0.9^\circ$ as a function of temperature.

the PD phase is much larger than that in the GD phase, showing stronger dynamic lattice distortion in the PD phase. The order parameter of the tilting $\langle \theta_i \tau_i \cdot \omega_{\text{ord}} \rangle$ is expected to be approximately proportional to the degree of the monoclinic lattice distortion corresponding to the strain e_4 (see Fig. 2). The reciprocal of the quantity defined by $\chi_{\theta\tau}(T) = (\langle \theta_i \tau_i \cdot \omega_{\text{ord}} \rangle^2 - \langle (\theta_i \tau_i \cdot \omega_{\text{ord}})^2 \rangle)/k_B T$ is therefore proportional to the elastic stiffness constant C_{44} . In Fig. 10(c), $1/\chi_{\theta\tau}(T)$ is plotted as a function of temperature. Both above and below T_N , $1/\chi_{\theta\tau}$ decreases

as temperature approaches to T_N . Since the transition is of the second order, the value of $1/\chi_{\theta\tau}$ is zero just at T_N . This temperature dependence of $1/\chi_{\theta\tau}$ is consistent with the behavior of C_{44} observed in ultrasonic wave velocity measurements¹¹⁾ and also in neutron scattering experiments¹²⁾ on Cr doped V_2O_3 , where C_{44} softens with decreasing temperature in the PI phase and approaches zero near the PI \rightarrow AFI transition temperature.

In Table III, spatial correlation functions $\langle \sigma_i \sigma_j \rangle$ and

Table III. Spatial correlation functions $\langle \sigma_i \sigma_j \rangle$ and $\langle \theta_i \tau_i \cdot \theta_j \tau_j \rangle$ between the first, second and third nearest neighbors along a lattice line are shown above and below the CO \rightarrow PD and CO \rightarrow GD phase transitions. In the CO phase, those along two different lattice lines, parallel and perpendicular to the ferromagnetic plane of the C-type AF order, are listed.

$C = 0.9^\circ, K/ J = 3.9^\circ, G/ J = 3$			
$k_B T/ J = 3.65^\circ$ (CO phase)			
	$\langle \sigma_i \sigma_j \rangle$	$\langle \theta_i \tau_i \cdot \theta_j \tau_j \rangle$	
1st	0.678	-0.735	1.21
2nd	0.670	0.702	1.07
3rd	0.681	-0.691	1.03
			1.16
			1.09
			1.05

$k_B T/ J = 3.9^\circ$ (PD phase)			
$\langle \sigma_i \sigma_j \rangle \quad \langle \theta_i \tau_i \cdot \theta_j \tau_j \rangle$			
1st	-0.191	0.170	
2nd	0.141	0.032	
3rd	-0.042	0.005	

$C = 1.8^\circ, K/ J = 3.9^\circ, G/ J = 3$			
$k_B T/ J = 3.3^\circ$ (CO phase)			
	$\langle \sigma_i \sigma_j \rangle$	$\langle \theta_i \tau_i \cdot \theta_j \tau_j \rangle$	
1st	0.964	-0.969	2.02
2nd	0.965	0.966	2.10
3rd	0.964	-0.965	2.07
			2.12
			2.04

$k_B T/ J = 3.8^\circ$ (GD phase)			
$\langle \sigma_i \sigma_j \rangle \quad \langle \theta_i \tau_i \cdot \theta_j \tau_j \rangle$			
1st	-0.957	-0.001	
2nd	0.955	0.007	
3rd	-0.955	-0.002	

$\langle \theta_i \tau_i \cdot \theta_j \tau_j \rangle$ between the first, second and third nearest neighbors along a lattice line are listed. Those for temperatures above and below the CO \rightarrow PD transition calculated with $C = 0.9^\circ$ are shown and for comparison, those for the CO \rightarrow GD transition calculated with $C = 1.8^\circ$ are also listed. In the CO phase, those along two different lattice lines, parallel and perpendicular to the ferromagnetic plane of the C-type AF order, are shown. In the PD phase, there is short range G-type AF spin correlation, which is consistent with recent neutron scattering experimental results.^{9, 10)} In addition to this, short range order of tilting directions is also present in this phase. This sudden change in the spin correlation, which is unusual for order-disorder magnetic transition can be explained as follows. In the PD phase, spins and the local lattice deformation are still dynamically coupled and short range C-type AF order with local lattice distortion survives. However, since the short range C-type AF order with three different directions of the ferromagnetic plane are coexistence, we find, in average, the G-type AF spin correlation as seen in Table III. In this way, the abrupt change in the spin correlation func-

tions observed at the AFI \rightarrow PI transition in the neutron scattering experiments is explained as a result of the simultaneous order to disorder transition of both the tilting directions and spins of the V ion pairs. On the other hand, in the GD phase, since lattice distortion is not required for the stabilization of the G-type AF spin order, the correlation functions between the tilting directions $\langle \theta_i \tau_i \cdot \theta_j \tau_j \rangle$ is almost zero. This is in contrast to the G-type AF spin correlation in the PD phase originating from the short range C-type AF order with the dynamic spin-lattice coupling.

§5. Resonant X-ray Scattering Analysis

Resonant x-ray scattering (RXS) has received much attention recently, as a technique for extracting direct information on magnetic^{33–35)} and orbital³⁶⁾ order. Possibility of observing the orbital ordering in V_2O_3 by RXS have been pointed out by Fabrizio *et al.*³⁷⁾ They made predictions on the light polarization and the azimuthal angle of the scattering plane dependence of the resonant Bragg reflection intensities, assuming the orbital order proposed by Castellani *et al.*¹³⁾ The RXS measurements on V_2O_3 ²⁰⁾ and its Cr doped alloys²¹⁾ have been performed by Paolasini *et al.* They insisted that in the AFI phase, there are resonant Bragg reflection peaks arising from the orbital ordering in addition to those caused by the AF magnetic ordering. On the other hand, Lovesey and Knight claimed that all these Bragg peaks can be attributed to the AF magnetic ordering and are associated with the orbital magnetic moment and the octupole moment of a V ion.²³⁾ In this section, discussion will be mainly focused on these resonant Bragg peaks, especially (111) reflection peak, whose origin is still controversial. It will be shown that the light polarization and the azimuthal angle dependence of the (111) Bragg reflection intensity can be explained within the V ion pair model and is attributed to not the orbital ordering but the antiferro (AF) magnetic ordering.

5.1 $1s \rightarrow 4p$ dipole X-ray scattering process

In this subsection, we will discuss the $1s \rightarrow 4p$ dipole process, which is dominant process in the RXS at the V K -edge absorption region. The x-ray scattering amplitude $f_{DD}(\omega)$ is expressed as

$$f_{DD}(\omega) = \sum_l e^{i(\mathbf{q}-\mathbf{q}') \cdot \mathbf{R}_l} (\mathbf{\epsilon}'^* \cdot \mathbf{F}^l(\omega) \mathbf{\epsilon}), \quad (7)$$

where \mathbf{q} and $\mathbf{\epsilon}$ are the wave vector and the polarization vector for the incoming photon, \mathbf{q}' and $\mathbf{\epsilon}'$ are those for the outgoing photon and \mathbf{R}_l denotes position of the l -th V ion site.

Here, the 3×3 tensor $\mathbf{F}^l(\omega)$ is defined by

$$\mathbf{F}^l(\omega) = q^2 \langle g | \mathbf{P} \frac{1}{E_g + \omega - H_m + i\Gamma_m/2} \mathbf{P} | g \rangle, \quad (8)$$

where $|g\rangle$ and E_g are the ground state wave functions and its energy, H_m and Γ_m are the Hamiltonian and a life-time term for the intermediate state reached by the $1s \rightarrow 4p$ transition and $\mathbf{P} = e\mathbf{r}$ is the electric dipole moment operator. Since delocalized feature of the $4p$

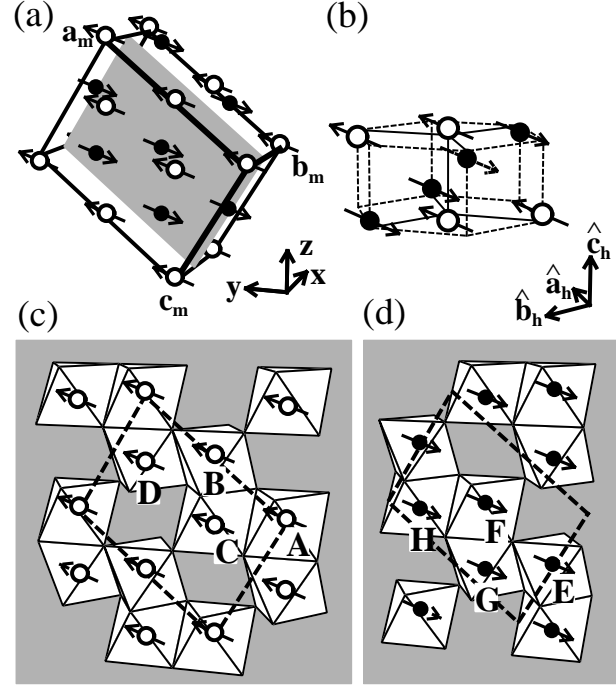


Fig. 11. Antiferromagnetic and crystal structures of V_2O_3 in the AFI phase. The white and black circles denote V ions and the arrows indicate direction of their magnetic moments. In (a), the monoclinic unit cell and the magnetic structure are shown. The magnetic moments are ferrromagnetically coupled in each monoclinic (010) layer, altering their direction between adjacent layers. The V ion pair and neighboring six V ions are depicted in (b). In (c) and (d), V ions belonging to two different (010) layers are separately depicted with surrounding oxygen octahedra.

orbital, the intermediate-state-multiplet dependence of RXS is not expected to be important. Thus, here we will consider the integrated value of $F^l(\omega)$ over the photon energy ω :

$$F_{i,j}^l = \int F_{i,j}^l(\omega) d\omega. \quad (9)$$

Note that $F_{x,x}^l$, $F_{y,y}^l$ and $F_{z,z}^l$ corresponds to the $1s \rightarrow 4p$ dipole transition probabilities integrated by ω at site l with x-, y- and z- linearly polarized light, respectively.

Before discussing rather complicate RXS in V_2O_3 , first of all, let us consider the most simplest antiferromagnet, where the unit cell with one magnetic ion site in the absence of magnetic order is doubled by the presence of the antiferromagnetic order and two magnetic sublattices A and B with opposite direction of the magnetic moment in each other are assumed. In this case, F^l for an ion site belongs to the sublattice A (here we denote it by F^A) can be obtained from that belongs to the sublattice B (denoted by F^B) by replacing the ground state wavefunction $|g\rangle$ in eq. (8) with $\Theta T|g\rangle$, where Θ represents the time reversal operator and T denotes the translation operator, which transforms ion sites belong to the sublattice A into those belong to the sublattice B. This

immediately leads to the relation:

$$F^A = F^{B*}.$$

For resonant Bragg reflection corresponding to the anti-ferromagnetic order, the integrated scattering amplitude f_{DD} is

$$\begin{aligned} f_{DD} &= \frac{N}{2} \sum_{i,j} (F_{i,j}^A - F_{i,j}^{A*}) \varepsilon_i \varepsilon_j' \\ &= iN \{ (\varepsilon_x \varepsilon_y' - \varepsilon_y \varepsilon_x') \text{Im}F_{x,y}^A + (\varepsilon_y \varepsilon_z' - \varepsilon_z \varepsilon_y') \text{Im}F_{y,z}^A \\ &\quad + (\varepsilon_z \varepsilon_x' - \varepsilon_x \varepsilon_z') \text{Im}F_{z,x}^A \}, \end{aligned} \quad (10)$$

where N denotes the number of the magnetic ion sites. $\text{Im}F_{x,y}^A$ can be written as

$$\text{Im}F_{x,y}^A = \frac{1}{2i} (F_{+1}^A - F_{-1}^A),$$

where $F_{\pm 1}^A$ are integrated transition probabilities of the $1s \rightarrow 4p$ dipole transition with plus and minus helicity light injected along the z -axis for an ion site belongs to the sublattice A. Carra *et al.* have proposed a sum rule for the core-level x-ray absorption spectra with the circularly polarized light.³⁸⁾ From the sum rule, it is easy to find that the quantity $F_{+1}^A - F_{-1}^A$ is proportional to the z -component of the orbital moment of the $4p$ orbital $\langle L_z^{4p} \rangle$ for a magnetic ion site belongs to the sublattice A in the ground state. Similarly, the quantities $\text{Im}F_{y,z}^A$ and $\text{Im}F_{z,x}^A$ are proportional to the x- and y-components of the $4p$ orbital angular momenta $\langle L_x^{4p} \rangle$ and $\langle L_y^{4p} \rangle$, respectively. The integrated amplitude f_{DD} is, therefore, proportional to $(\boldsymbol{\varepsilon} \times \boldsymbol{\varepsilon}') \cdot \langle \mathbf{L}^{4p} \rangle$.

In Fig. 11, the magnetic and crystal structures in the AFI phase are shown. The black and white circles are the V ion sites and the arrows indicate the direction of their magnetic moments. There are eight different V ion sites in the monoclinic unit cell shown in Fig. 11(a). In (b) and (c), two different (010) magnetic layers are separately drawn, and the eight V ion sites are labeled A to H. The integrated scattering amplitude $f_{DD}(h, k, l)$ of RXS at a (h, k, l) Bragg reflection can be written in the form:

$$\begin{aligned} f_{DD}(h, k, l) &= \frac{N}{8} \sum_{i,j} \varepsilon_i \varepsilon_j' [\{ F_{i,j}^A + (-)^{h+k+l} F_{i,j}^F \} \\ &\quad + \{ F_{i,j}^B + (-)^{h+k+l} F_{i,j}^E \} (-)^h \\ &\quad + \{ F_{i,j}^C + (-)^{h+k+l} F_{i,j}^H \} e^{i\alpha} \\ &\quad + \{ F_{i,j}^D + (-)^{h+k+l} F_{i,j}^G \} (-)^h e^{i\alpha}], \end{aligned} \quad (11)$$

where $\alpha \sim -4\pi(hx + lz)$. $x \sim 0.3438$ and $z \sim 0.2991$ are the position parameters of the V ions.²⁾ If we assume the antiferromagnetic structure above, the system is invariant under the symmetry operation $\{\Theta|\frac{1}{2}(\mathbf{a}_m + \mathbf{b}_m + \mathbf{c}_m)\}$ and by this operation, the V ion sites A, B, C and D are transformed into the sites F, E, H and G, respectively and as we have discussed above, relations $F^A = F^F$, $F^B = F^E$, $F^C = F^H$ and $F^D = F^G$ are satisfied. Similarly, the V ion sites A, C, E and G are transformed into the sites B, D, F and H by the $I2/a$ space group symmetry operation $\{\sigma_h|\frac{1}{2}\mathbf{a}_m\}$ and relations $F^A = F^B$, $F^C = F^D$, $F^E = F^G$ and $F^F = F^H$ are satisfied.

$F^C = F^D$, $F^E = F^F$ and $F^G = F^H$ are obtained. Using above relations among F^l 's and also the fact that the operation σ_h transforms $(\varepsilon_x, \varepsilon_y, \varepsilon_z)$ into $(\varepsilon_x, \varepsilon_y, -\varepsilon_z)$, we obtain the scattering amplitude for the reflections with $h = \text{even}$ and $h + k + l = \text{odd}$ as

$$\begin{aligned} f_{DD}(h, k, l) &= \\ &\quad \frac{iN}{2} \{ (\varepsilon_y \varepsilon_z' - \varepsilon_z \varepsilon_y') (\text{Im}F_{y,z}^A + e^{i\alpha} \text{Im}F_{y,z}^C) \\ &\quad + (\varepsilon_z \varepsilon_x' - \varepsilon_x \varepsilon_z') (\text{Im}F_{z,x}^A + e^{i\alpha} \text{Im}F_{z,x}^C) \}. \end{aligned} \quad (12)$$

On the other hand, the scattering amplitude for the reflections with $h = \text{odd}$ and $h + k + l = \text{odd}$ can be written as

$$\begin{aligned} f_{DD}(h, k, l) &= \\ &\quad \frac{iN}{2} (\varepsilon_y \varepsilon_z' - \varepsilon_z \varepsilon_y') (\text{Im}F_{y,z}^A + e^{i\alpha} \text{Im}F_{y,z}^C). \end{aligned} \quad (13)$$

It is obvious from eqs. (12) and (13) that the amplitudes are zero for the $\sigma\text{-}\sigma$ scattering, where the polarization vectors $\boldsymbol{\varepsilon}$ and $\boldsymbol{\varepsilon}'$ are perpendicular to the scattering plane and thus are parallel to each other. This is consistent with the experiments, where only vanishingly small intensities of both the (111) and (221) reflections for the $\sigma\text{-}\sigma$ scattering are observed.²⁰⁾ On the other hand, the $\sigma\text{-}\pi$ scattering, where one of the polarization vectors is perpendicular to the scattering plane and the other is in the plane, is not forbidden scattering and indeed, for the magnetic (221) Bragg reflection, strong RXS are observed in the experiment. The experimental $\sigma\text{-}\pi$ scattering at the (111) Bragg reflection, however, has only negligible small intensity in the $1s \rightarrow 4p$ excitation energy region. This fact can be explained as follows. Since the direction of the magnetic moment observed in the neutron experiment is almost in the $\mathbf{a}_m\text{-}\mathbf{b}_m$ plane, the x-component of the $4p$ orbital angular momentum $\langle L_x^{4p} \rangle$, which is perpendicular to the $\mathbf{a}_m\text{-}\mathbf{b}_m$ plane (see Fig. 11), is expected to be zero or small. Because eq. (13) only contains $F_{y,z}^A$ and $F_{y,z}^C$, which is proportional to $\langle L_x^{4p} \rangle$, the intensity should be almost zero.

5.2 Interference of $1s \rightarrow 4p$ and $1s \rightarrow 3d$ processes

We have discussed the $1s \rightarrow 4p$ dipole RXS. Only the dipole process, the scattering amplitude at the (111) Bragg reflection should be almost zero and thus the $1s \rightarrow 3d$ quadrupole transition expected to be important to explain the sharp peak observed at the prethreshold region. Since V^{3+} ion sites do not have inversion symmetry in V_2O_3 , the $4p$ and $3d$ orbitals on the same site can be hybridized in each other and this causes interference between the $1s \rightarrow 4p$ dipole transition and $1s \rightarrow 3d$ quadrupole transition processes.³⁷⁾ Because pure $1s \rightarrow 3d$ scattering amplitude is expected to be much smaller than the interference scattering amplitude, here, only this interference scattering process is considered.

The crystal field which causes the hybridization between the $4p$ and $3d$ orbitals in the same V ion site would be written as

$$V^l(\mathbf{r}) = \pm A_{1,0} r Y_{1,0}(\Omega) \pm A_{3,0} r^3 Y_{3,0}(\Omega)$$

$$\pm A_{3,3}r^3\{\text{Y}_{3,3}(\Omega) - \text{Y}_{3,-3}(\Omega)\}, \quad (14)$$

where the signs in front of three coefficients $A_{1,0}$, $A_{3,0}$ and $A_{3,3}$ depend on the sites: the plus signs in front of $A_{1,0}$ and $A_{3,0}$ are taken for A, B, E and F sites and the minus signs for the other sites and $+A_{3,3}$ for B, C, E and H sites and $-A_{3,3}$ for the others.

The relative values of the these three parameters were estimated using a VO₆ cluster model and they are $A_{3,3}/A_{3,0} = 0.79$ and $(A_{3,0}\langle 4p|r^3|3d\rangle)/(A_{1,0}\langle 4p|r|3d\rangle) \simeq -0.22$. If we take into account this hybridization as a second order perturbation with respect to V^l , we find for the interference term $f_{\text{DQ}}(\omega)$ as

$$\begin{aligned} f_{\text{DQ}}(\omega) = & i q^2 \sum_l e^{i(\mathbf{q}-\mathbf{q}') \cdot \mathbf{R}_l} \\ & \times \left[\langle g | D(\boldsymbol{\varepsilon}') \left(\frac{V^l}{\Delta_{4p-3d}} \right) \frac{1}{E_g + \omega - H_m + i\frac{\Gamma_m}{2}} Q(\boldsymbol{\varepsilon}, \mathbf{q}) | g \rangle \right. \\ & \left. - \langle g | Q(\boldsymbol{\varepsilon}', \mathbf{q}') \frac{1}{E_g + \omega - H_m + i\frac{\Gamma_m}{2}} \left(\frac{V^l}{\Delta_{4p-3d}} \right) D(\boldsymbol{\varepsilon}) | g \rangle \right], \end{aligned} \quad (15)$$

where $|g\rangle$ and E_g are the ground state wavefunction and its energy, $D(\boldsymbol{\varepsilon})$ and $Q(\boldsymbol{\varepsilon}, \mathbf{q})$ are the operators for the electric dipole and quadrupole transitions defined by $D(\boldsymbol{\varepsilon}) = e(\boldsymbol{\varepsilon} \cdot \mathbf{r})$ and $Q(\boldsymbol{\varepsilon}, \mathbf{q}) = e(\mathbf{r} \cdot \boldsymbol{\varepsilon})(\mathbf{r} \cdot \mathbf{q})$, Δ_{4p-3d} is the energy difference between the $4p$ and $3d$ levels and H_m and Γ_m are the Hamiltonian and the life-time term for the intermediate state reached by the $1s \rightarrow 3d$ excitation from the initial state.

The term $1/(E_g + \omega - H_m + i\Gamma_m/2)$ would be approximately replaced by $-i\pi \sum_\mu \delta(E_g + \omega - E_\mu) |\mu\rangle \langle \mu|$, where $H_m |\mu\rangle = E_\mu |\mu\rangle$ and with this approximation, the RXS amplitude integrated by ω over $1s \rightarrow 3d$ excitation energy region can be written as

$$\begin{aligned} & \int_{1s \rightarrow 3d} f_{\text{DQ}}(\omega) d\omega \\ & \sim \pi (eq)^2 \frac{\langle 1s | r | 4p \rangle \langle 1s | r^2 | 3d \rangle}{\Delta_{4p-3d}} \\ & \times \sum_{l,m,m'} e^{i(\mathbf{q}-\mathbf{q}') \cdot \mathbf{R}_l} \langle g | \sum_\sigma a_{lm\sigma} a_{lm'\sigma}^\dagger | g \rangle \\ & \times \left[D_m^*(\boldsymbol{\varepsilon}') V_{m,m'}^l Q_{m'}(\boldsymbol{\varepsilon}, \mathbf{q}) - Q_m^*(\boldsymbol{\varepsilon}', \mathbf{q}') V_{m',m}^{l*} D_{m'}(\boldsymbol{\varepsilon}) \right], \end{aligned} \quad (16)$$

where $V_{m,m'}^l = \int R_{4p}(r) Y_{1m}^*(\Omega) V^l(\mathbf{r}) R_{3d}(r) Y_{2m'}(\Omega) dr$ and $a_{lm\sigma}^\dagger$ denotes creation operator of an electron on the $3d$ orbital with magnetic m and spin σ quantum numbers on site l . D_m and Q_m are coefficients of the spherical expansions of the transition operators

$$\begin{aligned} D(\boldsymbol{\varepsilon}) &= er \sum_{m=-1}^1 D_m(\boldsymbol{\varepsilon}) Y_{1m}(\Omega) \\ Q(\boldsymbol{\varepsilon}, \mathbf{q}) &= er^2 \sum_{m=-2}^2 Q_m(\boldsymbol{\varepsilon}, \mathbf{q}) Y_{2m}(\Omega) \end{aligned}$$

and they are given by

$$\begin{aligned} D_{\pm 1} &= \sqrt{\frac{4\pi}{3}} \frac{\mp \varepsilon_x + i\varepsilon_y}{\sqrt{2}}, & D_0 &= \sqrt{\frac{4\pi}{3}} \varepsilon_z, \\ Q_{\pm 2} &= \sqrt{\frac{2\pi}{15}} \{ (q_x \varepsilon_x - q_y \varepsilon_y) \mp i(q_x \varepsilon_y + q_y \varepsilon_x) \}, \\ Q_{\pm 1} &= \sqrt{\frac{2\pi}{15}} \{ \mp (q_z \varepsilon_x + q_x \varepsilon_z) + i(q_y \varepsilon_z + q_z \varepsilon_y) \}, \\ Q_0 &= \sqrt{\frac{4\pi}{5}} q_z \varepsilon_z. \end{aligned}$$

The procedure of the calculations is following. Eight V ion sites (A to H in Fig. 11) in the monoclinic unit cell was considered to be four independent V ion pairs. For each of them, the ground state wavefunction was calculated using the V ion pair model described in § 2. In the calculations, molecular field $H_M = 0.01$ eV along the magnetic easy axis was applied so to reproduce experimentally observed antiferromagnetic order. Then, from the ground state wavefunctions, the quantity $\langle g | \sum_\sigma a_{lm\sigma} a_{lm'\sigma}^\dagger | g \rangle$ were calculated, and using eq. (16), the scattering amplitude was obtained.

5.3 Analysis of the (111) Bragg reflection

Figure 12 shows the theoretical azimuthal angle Φ de-

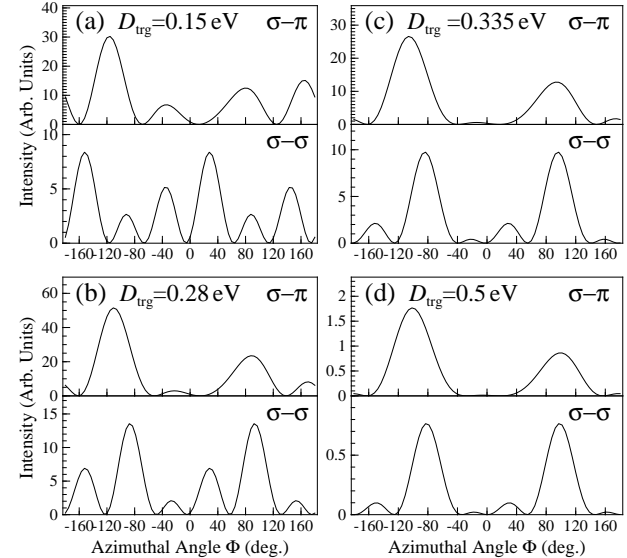


Fig. 12. Azimuthal angle dependence of the integrated intensities for the (111) Bragg reflection in the AFI phase calculated with various values of the trigonal crystal field D_{trg} . Intensities for the two polarization conditions $\sigma\text{-}\sigma$ and $\sigma\text{-}\pi$ calculated with the parameters $D_{\text{trg}} = 0.15$ eV (a), $D_{\text{trg}} = 0.28$ eV (b), $D_{\text{trg}} = 0.335$ eV (c) and $D_{\text{trg}} = 0.5$ eV (d).

pendence of the integrated intensities for the (111) Bragg reflection in the AFI phase for various values of D_{trg} . The intensities with the two polarization conditions $\sigma\text{-}\sigma$ and $\sigma\text{-}\pi$ calculated with the parameters $D_{\text{trg}} = 0.15$ eV (a), $D_{\text{trg}} = 0.28$ eV (b), $D_{\text{trg}} = 0.335$ eV (c) and $D_{\text{trg}} = 0.5$ eV (d) are shown. The scattering plane is parallel to

the z -axis at $\Phi = 0$. The tilting angle of the magnetic moment θ_M in the ground state with $D_{\text{trg}} = 0.15$ eV, 0.28 eV, 0.335 eV and 0.5 eV are $\theta_M = 16^\circ, 51^\circ, 71^\circ$ and 84° , respectively.

It is seen in the figure that the azimuthal angle Φ dependence of the scattering intensities are strongly influenced by the direction of the orbital magnetic moment. The intensity curve in Fig. 12(c) with $\theta_M = 71^\circ$, which is the same angle observed in the neutron diffraction experiment⁸⁾ and Fig. 12(b) with $\theta_M = 51^\circ$ are most resemble to the experimental intensity curve in ref. 20. On the other hand, the curve in Fig. 12(b), where $\theta_M = 16^\circ$ and the ground state is almost pure $e^\pi a_1; e^\pi e^\pi (e^\pi e^\pi; e^\pi a_1)$ state, is very different from experimental one. This indicates that the experimental results are well explained with the $e^\pi e^\pi; e^\pi e^\pi$ and $e^\pi a_1; e^\pi e^\pi$ mixed ground state and consistent with the present theory. It is also important to mention that if the spin-orbit interaction is switched off, the scattering intensity is zero for this reflection, although there exists the molecular ferro-orbital order in the ground state. The reflection, therefore, originates from not the molecular ferro-orbital order but the AF magnetic order.

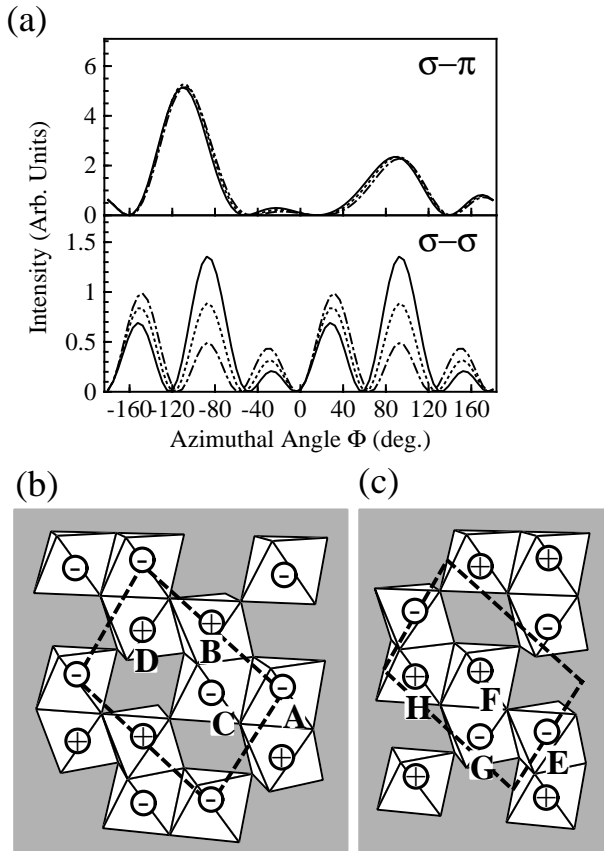


Fig. 13. In (a), azimuthal angle dependence of the integrated intensities for the (111) reflection in the AFI phase calculated with $C_A(e_u^\pi, e_v^\pi) = -0.02$ eV (solid line), 0.0 eV (dashed line) and 0.02 eV (dotted-dashed line) are shown. In (b) and (c), the same as Fig. 11 (c) and (d), the sign (\pm) of M_{Lx} on V ions are shown.

The scattering intensity is also sensitive to a small x-component of the orbital magnetic moment M_{Lx} . Possibility of the presence of such small x-component of the magnetic moment was pointed out by Moon.⁸⁾ M_{Lx} can be induced by the low symmetry crystal field $C_A(e_u^\pi, e_v^\pi)$. In Fig. 13(a), Φ dependence of the integrated intensities for the (111) reflection obtained with $C_A(e_u^\pi, e_v^\pi) = -0.02$ eV (solid line), 0 eV (dashed line) and 0.02 eV (dotted-dashed line) are drawn. $D_{\text{trg}} = 0.28$ eV is adopted. In Figs. 13(b) and (c), the sign of M_{Lx} on each V ion for $C_A(e_u^\pi, e_v^\pi) < 0$ is shown for the two magnetic layers in Figs. 11(b) and (c). For $C_A(e_u^\pi, e_v^\pi) > 0$, all the signs of M_{Lx} are altered. As seen in the Fig. 13(a), the $\sigma-\sigma$ scattering intensity is strongly influenced by the value of $C_A(e_u^\pi, e_v^\pi)$, although the magnitude of M_{Lx} induced by $C_A(e_u^\pi, e_v^\pi) = \pm 0.02$ eV is an order of $\sim 0.01 \mu_B$. With $C_A(e_u^\pi, e_v^\pi) = 0.02$ eV the calculated intensity curve is not resemble to the experimental one whereas with $C_A(e_u^\pi, e_v^\pi) = -0.02$ eV, good agreement with experimental intensity curve is achieved.

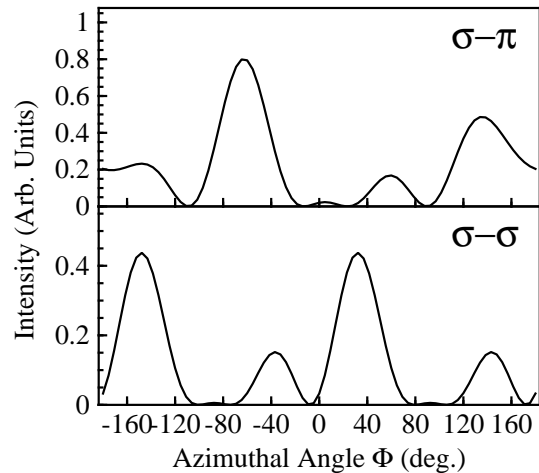


Fig. 14. Azimuthal angle dependence of the integrated intensity for the (111) reflection in the AFI phase calculated with $D_{\text{trg}} = 0.28$ eV. The $1s \rightarrow 3d$ quadrupole transition instead of the $1s \rightarrow 3d$ and $1s \rightarrow 4p$ interference process is assumed as for the RXS process.

Lovesey and Knight argued that the (111) reflection peak can be explained by pure $1s \rightarrow 3d$ quadrupole transition.²³⁾ Contrary to this, in the presence theory, the peak is attributed to the interference process of the $1s \rightarrow 4p$ dipole and $1s \rightarrow 3d$ quadrupole transitions. For comparison, in Fig. 14, Φ dependence of the scattering intensity of the (111) reflection peak obtained with the pure $1s \rightarrow 3d$ quadrupole transition instead of the interference process is shown. The intensity curve calculated with $D_{\text{trg}} = 0.28$ eV is very different from experimental curve. Results obtained with other parameter values of D_{trg} and $C_A(e_u^\pi, e_v^\pi)$ also does not agree with experimental intensity curve.

§6. Linear Dichroism in V 2p XAS

In this section, the dependence of the V 2p XAS spectra on the polarization vector ϵ of the light will be discussed. As was mentioned in the previous sections, such experiment was already done by Park *et al.*¹⁴⁾ with the polarization vectors ϵ being parallel and perpendicular to the c_h axis. Because of the selection rule of the $2p \rightarrow 3d$ dipole transition, the transition probability to the a_1 orbital is larger than that to the e^π orbital for $\epsilon \parallel c_h$, whereas that to the e^π orbital is larger for the $\epsilon \perp c_h$. Thus the difference spectrum is sensitive to the $e^\pi a_1$ to $e^\pi e^\pi$ occupation ratio in the initial state. The ratio was deduced from the experiment using a VO_6 cluster model and was found to be $e^\pi a_1 : e^\pi e^\pi \sim 1 : 1$ for the PM phase and $e^\pi a_1 : e^\pi e^\pi \sim 1 : 2$ for the AFI phase.

To verify the present theory, the spectra was calculated using the V ion pair model described in § 2.1. For the initial state, the ground state of the V ion pair model is assumed. For the final state, the configurations $2p3d^3; 3d^2$, $2p3d^1; 3d^3$ and $2p3d^4; 3d^1$ are considered, where $2p$ denotes a hole on the V 2p orbital in one of the V ion site. In addition to the interactions considered in the Hamiltonian described in § 2.1, the $3d$ - $2p$ multipole interaction and the $2p$ spin-orbit interaction are also included in the calculation of the final states.³⁹⁾ The $2p \rightarrow 3d$ dipole transition is considered as the photoprocess and the intensities of the spectra $I_\kappa(\omega)$ as a function of the incident photon energy ω is written as

$$I_\kappa(\omega) \propto \sum_f |\langle f | T_\kappa | g \rangle|^2 \delta(E_g + \omega - E_f) \\ = \lim_{\delta \rightarrow 0} \frac{-1}{\pi} \text{Im} \langle g | T_\kappa^\dagger \frac{1}{E_g + \omega - H_f + i\delta} T_\kappa | g \rangle, \quad (17)$$

where $|f\rangle$, E_f and H_f denote the wavefunction, eigen energy and Hamiltonian of the final state, respectively, T_κ represents the $2p \rightarrow 3d$ dipole transition operator and κ specifies the polarization direction of the linearly polarized light. The spectra was calculated using the recursion method⁴⁰⁾ and a Lorentzian broadening was further applied the spectra.

The parameters used in the calculations are the same to those listed in Table II and $D_{\text{trg}} = 0.28$ eV is adopted. In the final state, there are additional parameters related to the $2p$ core-hole: the $3d$ - $2p$ Coulomb repulsion energy $U_{dp} = 3.07$ eV, the $2p$ spin-orbit interaction $\zeta_p = 4.649$ eV, the $3d$ - $2p$ Slater integrals $F_{dp}^2 = 4.361$ eV, $G_{dp}^1 = 3.162$ eV and $G_{dp}^3 = 1.797$ eV.

Figure 15 shows the calculated spectra obtained using the V ion pair model with the polarization vectors ϵ parallel and perpendicular to the c_h axis. In Fig. 15(a) the spectra for the PM phase, and in Fig. 15(b) those for the AFI phase are shown and in each panel, the difference spectrum is also depicted. The theoretical spectra well reproduce experimental ones especially those for the AFI phase in ref. 14. Although the difference spectrum for the PM phase is less similar to the experimental one, its tendency to have negative peaks at -7 eV and 0 eV is consistent with the experiment. The polarization of the spectra defined by $P = (I_{\parallel} - I_{\perp})/(I_{\parallel} + I_{\perp})$ are $P = 0.027$ for the AFI phase and $P = 0.015$ for the PM phase,

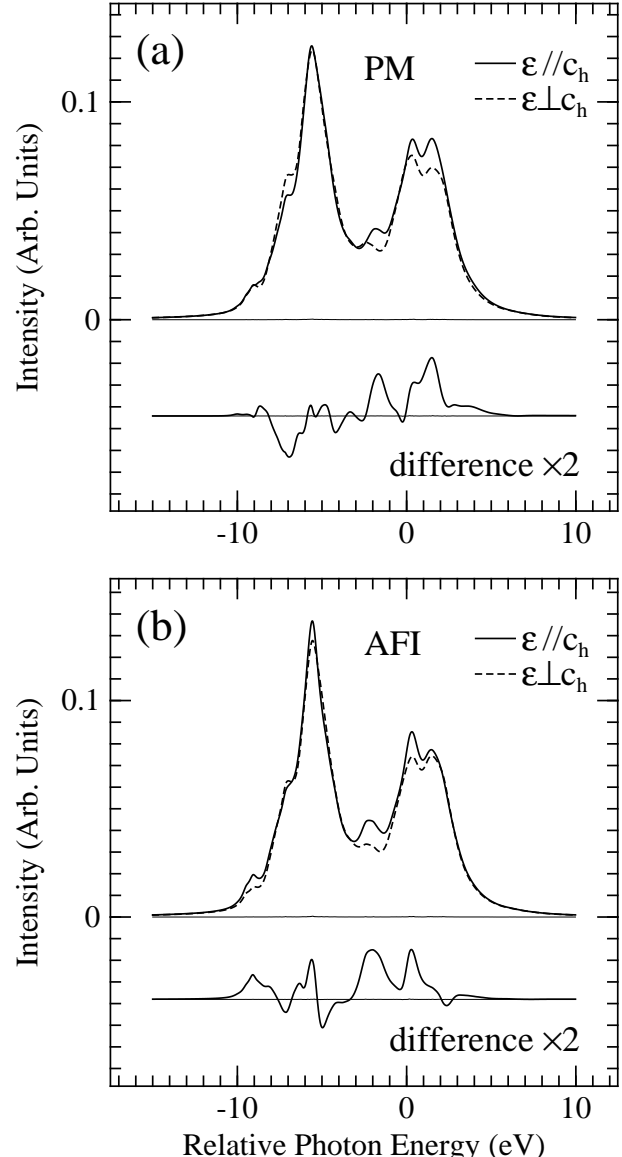


Fig. 15. Theoretical polarization-dependent V 2p XAS spectra for V_2O_3 for the PM (a) and AFI (b) phases. The spectra are depicted for two different directions of the polarization vectors ϵ of the light: parallel and perpendicular to the c_h axis. The difference spectra are also shown below in each panel.

where I_{\parallel} and I_{\perp} denote integrated intensity of the spectra with the light polarization parallel and perpendicular to the c_h axis, respectively. Such large change in the polarization between the two phases is also consistent with the experiment. Note that although the electron occupation of the e^σ orbitals in the ground state is small $\sim 5\%$, the inclusion of the e^σ orbital is important to reproduce the spectra, especially its polarization.

The sensitivity of the V 2p XAS spectra with polarized light to the orbital occupation in the initial state is useful to ascertain whether the orbital order exists or not in the AFI phase. To demonstrate this, in Fig. 16 the polarization-dependent V 2p XAS spectra are shown for two different direction of ϵ in the plane which is per-

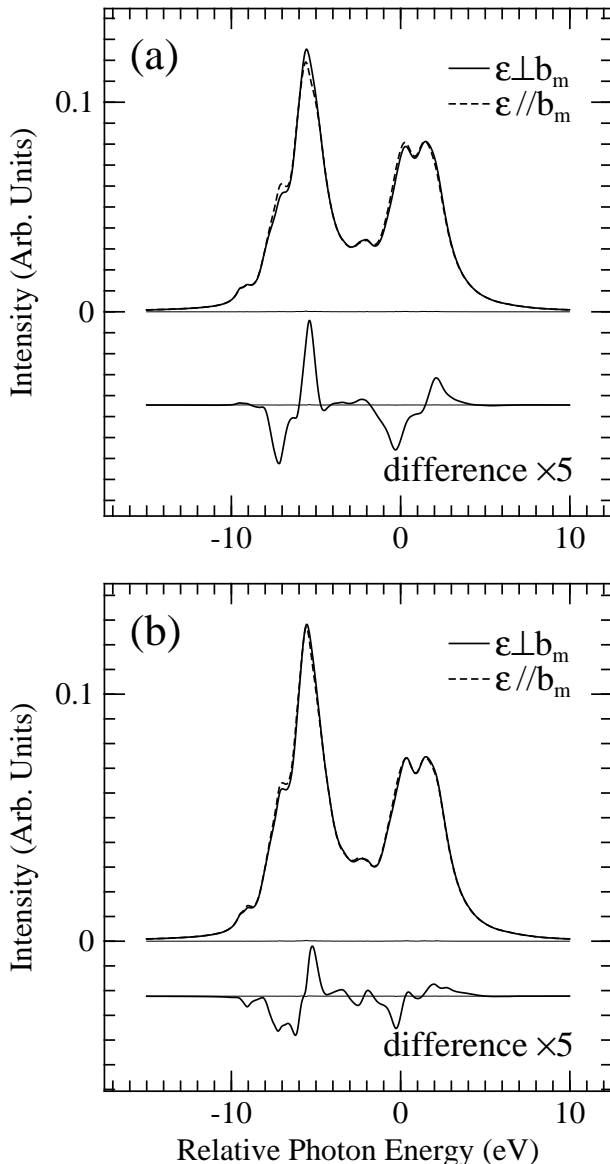


Fig. 16. Theoretical polarization-dependent V 2p XAS spectra for the AFI phase calculated without (a) and with (b) the 3d spin-orbit interaction. $D_{\text{trg}} = 0.28$ eV is assumed. The spectra are depicted for two different directions of the polarization vectors ϵ of the light: parallel and perpendicular to the monoclinic \mathbf{b}_m axis. The difference spectra are also shown below in each panel.

perpendicular to the \mathbf{c}_h axis: $\epsilon \perp \mathbf{b}_m$ and $\epsilon // \mathbf{b}_m$. The spectra without (a) and with (b) the 3d spin-orbit interaction is presented; other parameters are the same to those adopted for the AFI phase. The difference spectra are also shown below in each panel.

As was discussed in § 2.3, in the absence of the 3d spin-orbit interaction, the ground state has an orbital polarization corresponding to the molecular ferro-orbital ordering state of Mila's model (Fig. 16(a)). On the other hand, in the presence of the spin-orbit interaction, the ground state has no orbital ordering and instead of this a large orbital magnetic moment is induced in the

ground state (Fig. 16(b)). The magnitude of the difference spectrum in Fig. 16(a) is much larger than that in Fig. 16(b) and the shape of the spectrum in Fig. 16(a) largely vary from that in Fig. 16(b). Thus the measurement of this linear dichroic V 2p spectra, will be a crucial check whether the large orbital moment is present or not.

§7. Conclusions

The 3d electronic structure and phase transition in pure and Cr doped V_2O_3 were theoretically investigated in relation to the 3d spin-orbit interaction and lattice distortion. The 3d electronic state of V_2O_3 have been discussed, using a V ion pair model on the basis of the configuration interaction approach. In the model, the 3d-3d multipole interaction, a trigonal crystal field and the 3d spin-orbit interaction were considered and electron hopping between nearest neighbor V ions was also taken into account. In the presence of the 3d spin-orbit interaction, spin and orbital degrees of freedom are strongly coupled and this removes the orbital degeneracy of the ground state, resulting in no orbital ordering. Instead of this, each V ion with $S = 1$ spin state has a large orbital magnetic moment $\sim 0.7\mu_B$ in the AFI phase. These results are in contrast to those obtained from the similar V ion pair model proposed by Mila *et al.*, in which a ferro molecular orbital ordering occurs in the AFI phase.^{18, 19)} The large orbital moment is in accordance with the ratio $M_L/M_S \sim -0.3$ deduced from the nonresonant magnetic x-ray scattering experiment²⁰⁾ and also explains small total magnetic moment $1.2\mu_B$ observed in the AFI phase.⁸⁾ Because of the presence of the large orbital magnetic moment, the monoclinic lattice distortion and the direction of the magnetic easy axis is strongly connected in the AFI phase. The direction of magnetic moment was found to be canted from the corundum \mathbf{c}_h -axis in the presence of the monoclinic distortion and this agrees with the neutron diffraction experiments.⁸⁾

The local lattice distortion energy due to tilting of the V ion pair from the corundum c -axis was further considered. From the present model, it is expected that there is at least two local minima for the free energy in the real system as a function of the V-V distance of the pair. One is positioned at the V-V distance in the PM phase, where the energy difference of the two kinds of the state $e^\pi a_1; e^\pi e^\pi$ and $e^\pi e^\pi; e^\pi a_1$ is large and thus no electron-lattice coupling takes place. The electronic state of the V ion pair in this phase is described as a superposition of two configurations $e^\pi a_1; e^\pi e^\pi$ and $e^\pi e^\pi; e^\pi a_1$ in equal weight, which is similar to Mila's model. The other one is located at the V-V distance in the PI and AFI phases, where energies of the two kinds of the states are degenerate and Jahn-Teller like lattice distortion is the cause of the energy lowering at this V-V distance. Because of the tilting of the V ion pair caused by this lattice instability, the $e^\pi e^\pi; e^\pi e^\pi$ state is further hybridized with above $e^\pi a_1; e^\pi e^\pi$ ($e^\pi e^\pi; e^\pi a_1$) state in these phases. This large difference in the electron occupation between the metal and insulating phases agrees with the recent linear dichroic V 2p x-ray absorption spectroscopy (XAS) experimental results.¹⁴⁾

Since both in the AFI and PI phases, the electron-

lattice coupling strongly influences the orbital occupation and charge fluctuation, the PM \rightarrow AFI and PM \rightarrow PI transitions can not be regarded as usual Mott transition. The elongation of the V-V distance and resultant reduction in the hybridization strength between the 3d orbitals caused by this electron-lattice coupling is probably responsible for these metal-insulator transitions.

To investigate interplay between magnetic ordering and the lattice distortion, an effective spin Hamiltonian including the effects of tilting of the V ion pairs was introduced. The antiferromagnetic order with the monoclinic lattice distortion observed in the AFI phase was reproduced in this model, where simultaneous ordering of the tilting directions and the magnetic moments of the V ion pairs take place. With increasing temperature, it exhibits antiferromagnetic to paramagnetic phase transition corresponding to the AFI \rightarrow PI transition in the real system. While all V ion pairs are tilted to the same direction and this gives rise the monoclinic lattice distortion in the AFI phase, their tilting directions are disordered and fluctuate among the three stable directions in the PI phase. As a result, there is no monoclinic distortion in the PI phase. It was also found that the C_{44} elastic constant softens and short-range spin correlation functions abruptly changes at this second order transition in this model. These results are consistent with the ultrasonic-wave measurement¹¹⁾ and recent neutron scattering experiments.^{9, 10)}

To confirm the validity of the present model, recent experiments on the resonant X-ray scattering (RXS) at the V K -edge^{20, 21)} and the linear dichroic V 2p XAS experiments¹⁴⁾ were analyzed. The (111) Bragg reflection observed in the RXS experiments, particularly in its azimuthal angle and polarization dependence of the 1s \rightarrow 3d peak, is well explained within the present model, where no orbital ordering is present and the antiferromagnetic order is assumed. The reflection is pure magnetic and the scattering amplitude of this reflection mainly arises from the interference process of the 1s \rightarrow 4p dipole and 1s \rightarrow 3d quadrupole transitions. The shape and magnitude of the linear dichroic V 2p XAS spectra in both the AFI and PM phases are well reproduced within the present model. Another linear dichroic V 2p XAS experiment has been proposed, which is sensitive to the presence of the orbital order in the initial state and will be a crucial check to the present model.

This work is partly supported by a Grant-in-Aid for Scientific Research from the Ministry of Education, Culture, Sports, Science and Technology.

- 1) N. F. Mott: *Metal Insulator Transitions* (Taylor & Francis, London, 1974).
- 2) P. D. Dernier and M. Marezio: Phys. Rev. B **2** (1970) 3771.
- 3) D. B. McWhan and J. P. Remeika: Phys. Rev. B **2** (1970) 3734.
- 4) A. Jayaraman, D. B. McWhan, J. P. Remeika and P. D. Dernier: Phys. Rev. B **2** (1970) 3751.
- 5) A. Menth and J. P. Remeika: Phys. Rev. B **2** (1970) 3756.
- 6) D. B. McWhan, A. Menth, J. P. Remeika, W. F. Brinkman and T. M. Rice: Phys. Rev. B **7** (1973) 1920.
- 7) H. Kuwamoto, J. M. Honig and J. Appel: Phys. Rev. B **22** (1980) 2626.

- 8) R. M. Moon: Phys. Rev. Lett. **25** (1970) 527; J. Appl. Phys. **41** (1970) 883.
- 9) W. Bao, C. Broholm, G. Aeppli, P. Dai, J. M. Honig and P. Metcalf: Phys. Rev. Lett. **78** (1997) 507.
- 10) W. Bao, C. Broholm, G. Aeppli, S. A. Carter, P. Dai, T. F. Rosenbaum, J. M. Honig, P. Metcalf and S. F. Trevino: Phys. Rev. B **58** (1998) 12727.
- 11) H. Yang, R. J. Sladek and H. R. Harrison: Solid State Commun. **47** (1983) 955.
- 12) M. Yethiraj, S. A. Werner, W. B. Yelon and J. M. Honig: Phys. Rev. B **36** (1987) 8675.
- 13) C. Castellani, C. R. Natoli and J. Ranninger: Phys. Rev. B **18** (1978) 4945; *ibid* B **18** (1978) 4967.
- 14) J.-H. Park, L. H. Tjeng, A. Tanaka, J. W. Allen, C. T. Chen, P. Metcalf, J. M. Honig, F. M. F. de Groot and G. A. Sawatzky: Phys. Rev. B **61** (2000) 11506.
- 15) V. I. Anisimov, J. Zaanen and O. K. Andersen: Phys. Rev. B **44** (1991) 943.
- 16) V. I. Anisimov, F. Aryasetiawan and A. I. Liechtenstein: J. Phys.: Condens. Matter **9** (1997) 767.
- 17) S. Yu. Ezhov, V. I. Anisimov, D. I. Khomskii and G. A. Sawatzky: Phys. Rev. Lett. **83** (1999) 4136.
- 18) F. Mila, R. Shiina, F.-C. Zhang, A. Joshi, M. Ma, V. Anisimov and T. M. Rice: Phys. Rev. Lett. **85** (2000) 1714.
- 19) R. Shiina, F. Mila, F.-C. Zhang and T. M. Rice: Phys. Rev. B **63** (2001) 144422.
- 20) L. Paolasini, C. Vettier, F. de Bergevin, F. Yakhou, D. Maninx, A. Stunault, W. Neubeck, M. Altarelli, M. Fabrizio, P. A. Metcalf and J. M. Honig: Phys. Rev. Lett. **82** (1999) 4719.
- 21) L. Paolasini, S. Di Matteo, C. Vettier, F. de Bergevin, A. Sollier, W. Neubeck, F. Yakhou, P. A. Metcalf and J. M. Honig: J. Elect. Spectr. Relat. Phenom. **120** (2001) 1.
- 22) J. W. Allen: Phys. Lett. **36** (1976) 1249.
- 23) S. W. Lovesey and K. S. Knight: J. Phys.: Condens. Matter **12** (2000) L367.
- 24) A. Tanaka and T. Jo: J. Phys. Soc. Jpn. **63** (1994) 2788.
- 25) H. Eskes and G. A. Sawatzky: Phys. Rev. B **43** (1991) 119.
- 26) A. Tanaka and T. Jo: J. Phys. Soc. Jpn. **65** (1996) 912.
- 27) S. Sugano, Y. Tanabe and H. Kamimura: *Multiplets of Transition-Metal Ions in Crystal* (Academic Press, New York, 1970).
- 28) A. E. Bocquet, T. Mizokawa, K. Morikawa, A. Fujimori, S. R. Barman, K. Maiti, D. D. Sarma, Y. Tokura and M. Onoda: Phys. Rev. B **53** (1996) 1161.
- 29) T. Uozumi, K. Okada, A. Kotani, R. Zimmermann, P. Steiner, S. Hüfner, Y. Tezuka and S. Shin: J. Elect. Spectr. Relat. Phenom. **83** (1997) 9.
- 30) T. Uozumi, K. Okada and A. Kotani: J. Elect. Spectr. Relat. Phenom. **78** (1996) 103.
- 31) W. A. Harrison: *Electronic Structure and Physical Properties of Solids* (Freeman, San Francisco, 1980).
- 32) T. M. Rice: *Spectroscopy of Mott Insulators and Correlated Metals*, edited by A. Fujimori and Y. Tokura (Springer, Berlin, 1995).
- 33) Doon Gibbs, D. R. Harshman, E. D. Isaacs, D. B. McWhan, D. Mills and C. Vettier: Phys. Rev. Lett. **61** (1988) 1241.
- 34) J. P. Hannon, G. T. Trammell, M. Blume and Doon Gibbs: Phys. Rev. Lett. **61** (1988) 1245.
- 35) D. B. McWhan, C. Vettier, E. D. Isaacs, G. E. Ice, D. P. Siddons, J. B. Hastings, C. Peters and O. Vogt: Phys. Rev. B **42** (1990) 6007.
- 36) K. Hirota, N. Oumi, T. Matsumura, H. Nakao, Y. Wakabayashi, Y. Murakami and Y. Endoh: Phys. Rev. Lett. **84** (2000) 2706.
- 37) M. Fabrizio, M. Altarelli and M. Benfatto: Phys. Rev. Lett. **80** (1998) 3400; *ibid* **81** (1998) 4030.
- 38) P. Carra, B. T. Thole, M. Altarelli and X. Wang: Phys. Rev. Lett. **70** (1993) 694.
- 39) A. Tanaka and T. Jo: J. Phys. Soc. Jpn. **61** (1992) 2040.
- 40) R. Haydock, V. Heine and M. J. Kelly: J. Phys. C **5** (1972) 2845.